THE ASTROPHYSICAL JOURNAL, 448:748–765, 1995 August 1

DOES NEAR-INFRARED POLARIMETRY REVEAL THE MAGNETIC FIELD IN COLD DARK CLOUDS?

ALYSSA A. GOODMAN[1,2,3,4]
Department of Astronomy, Harvard University, 60 Garden Street, Cambridge, MA 02138
TERRY J. JONES[2]
School of Physics and Astronomy, University of Minnesota, 116 Church Street, S.E., Minneapolis, MN 55455
ELIZABETH A. LADA[1,5]
Department of Astronomy, University of Maryland, College Park, MD 20742; and Harvard-Smithsonian Center for Astrophysics
AND
PHILIP C. MYERS[2]
Harvard-Smithsonian Center for Astrophysics, 60 Garden Street, Cambridge, MA 02138
Received 1994 November 1; accepted 1995 February 13

ABSTRACT

We present near-infrared (*JHK*) observations of the polarization of background starlight seen through the filamentary dark cloud L1755. The mean position angle and dispersion of the polarization vectors measured in the near-infrared, for stars along lines of sight passing *through* the densest portions ($1 < A_V < 10$ mag) of L1755, are virtually identical to those in an optical polarization map of stars around the *periphery* ($A_V \sim 1$ mag) of L1755. Furthermore, the percentage of polarization is not seen to increase, at all, with extinction in the near-infrared observations. We surmise that much of the dust in the dark cloud is *extinguishing* background starlight significantly, but not *polarizing* it efficiently, and thus that the *polarization map of background starlight cannot reliably trace the magnetic field associated with the dense interior of the dark cloud.* Our results in L1755 are remarkably similar to what we found in the dark cloud B216-217 (Goodman et al. 1992), which also shows no change in the polarization map associated with the cloud, and no rise in percentage polarization with extinction.

Using our multiwavelength polarimetric observations of L1755, we have estimated the wavelength of maximum polarization, λ_{max}, for most of the 53 stars in our sample. We find an unusually broad distribution of λ_{max}, with a mean at 0.88 ± 0.34 μm. The large range of λ_{max} leads us to the hypothesis that there is a wide range of grain sizes and/or shapes along the lines of sight through L1755. We conclude that only a small subset of grains is responsible for producing the polarization of background starlight, and that these grains may be critically underrepresented in the dense interiors of cold dark clouds.

Subject headings: dust, extinction — infrared: ISM: continuum — ISM: clouds — ISM: individual (L1755) — ISM: magnetic fields — polarization

1. INTRODUCTION

Forty-five years ago, Hall and Hiltner and their collaborators discovered that the light from stars can appear polarized when observed from the Earth (Hall 1949; Hall & Mikesell 1949, 1950; Hiltner 1949a, b, 1950). Soon after this discovery, Davis & Greenstein (1951) theorized that the observed polarization is caused by dust grains along the line of sight which have been oriented by an interstellar magnetic field. This explanation is now widely accepted, and maps of the polarization of background starlight are usually presumed to be maps of the interstellar magnetic field between the observer and the background stars, as projected onto the plane of the sky.

Dust grains are most effective at polarizing light whose wavelength is similar to the size of an individual grain. Thus, the percentage of polarization observed for background stars should, and does, depend on wavelength (Serkowski, Mathewson, & Ford 1975; Wilking et al. 1980). The maximum polarization occurs near 6000 Å for many lines of sight through the interstellar medium (ISM). So, primarily in the interest of expediency, most background starlight polarization maps are made at a reddish visual wavelength in order to optimize the product of a background star's brightness and its polarization. In regions of high dust column density (visual extinction $A_V \gg 1$ mag), It is not possible to "see" background stars at visual wavelengths, so many polarimetric studies of background starlight seen through dense clouds have been carried out at near-infrared wavelengths (Wilking et al. 1979; Hodapp 1984, 1987a, b, 1990; Sato et al. 1988; Tamura et al. 1987, 1988; Goodman et al. 1992, hereafter Paper I; Jones, Hyland, & Bailey 1984; Klebe & Jones 1990), where dust produces less extinction by a factor of ~ 10. It was the aim of most of these studies to determine magnetic field structure in these dense regions.

Our original aim in the research described in this paper and in Paper I was to study the magnetic field structure associated with *elongated dark clouds in star-forming regions.* The typical particle density in these dark clouds is $\sim 10^3$ cm^{-3} on a scale

[1] Visiting Astronomer at the Kitt Peak National Observatory, operated by the Association of Universities for Research in Astronomy, Inc., under contract with the National Science Foundation.
[2] Visiting Astronomer at the Infrared Telescope Facility, which is operated by the University of Hawaii under contract to the National Aeronautics and Space Administration.
[3] Alfred P. Sloan Fellow.
[4] NSF Young Investigator.
[5] NASA Hubble Fellow.

of ~0.5 pc, rendering them visually opaque. So, in maps of the polarization of background starlight made at visual wavelengths, these "dark" regions appear as nearly empty holes in the polarization map. In principle, one can fill in the hole corresponding to a dark cloud by observing background stars at longer (near-infrared) wavelengths where the cloud is more transparent and the polarization of background starlight is still appreciable.

In Paper I, we presented maps of the polarization of near-infrared background starlight in the dark cloud Barnard 216-217 (B216-217) in Taurus, and here we present results for the Lynds 1755 (L1755) dark cloud in Ophiuchus. Optical polarization maps using stars around the periphery of these dark clouds, with "holes" in the highest column density regions, had been made prior to our infrared observations. As seen in projection onto the plane of the sky, in B216-217, the optical polarimetry implies a field direction *perpendicular* to the long axis of the dark cloud (Heyer et al. 1987), and in L1755 the optical polarimetry implies a field *along* the long axis of the cloud (Goodman et al. 1990). These two cases represent the two extremes of possible projected field/cloud orientation, and it should be noted that in general, the orientation of elongated dark clouds with respect to field directions implied by optical polarimetry appears to be random (Goodman et al. 1990; Myers & Goodman 1991, hereafter MG). This lack of a general correlation between the direction of cloud elongation and magnetic field orientation implied by the polarization of background starlight seen through the periphery of dark clouds was the primary motivation behind our attempts to investigate the field structure "deeper" inside dark clouds with infrared polarimetry. Perhaps, we thought, if we could somehow see "inside" the dark cloud, the relation between density structure and field structure would become more apparent.

In B216-217, the near-infrared polarization observed along lines of sight "through" the dark cloud has the same mean direction and dispersion as the optical polarization observed around the cloud's periphery. Furthermore, the polarization efficiency (ratio of polarization to extinction, p/A_V) appears to decrease as extinction increases, so that virtually no rise in polarization is seen with increasing extinction in B216-217. In less elongated dark clouds, similar but somewhat less drastic drops in p/A_V as a function of A_V have also been noted (Wilking et al. 1979; Montei et al. 1984; Tamura et al. 1987; Vrba, Coyne, & Tapia 1981). In Paper I, we favor a true decrease in the polarizing effectiveness of the grains inside dark clouds, rather than geometric effects, as the cause of the drop in p/A_V.

In § 3 of this paper, we present the results of our near-infrared polarimetric observations of stars behind L1755. The observations show that the mean position angle and dispersion of the near-infrared polarization vectors (associated with the dense part of the dark cloud) and the optical polarization vectors (around the cloud's periphery) are nearly identical. And the percentage polarization appears to be independent of extinction. These two results are very similar to what we found in B216-217 (Paper I). Thus, the only striking difference between the polarization maps of these two dark clouds is that in B216-217 the means polarization direction is perpendicular to the cloud's long axis, and in L1755 it is parallel. In L1755, where we have carried out multiwavelength observations for most of the stars in the polarization map, the wavelength dependence of the polarization observed implies an unusually large range of λ_{max}, the wavelength of maximum polarization (§ 3.2.3).

We infer from our data that observed polarization at both optical and near-infrared wavelengths is due mostly to a particular population (of elongated, aligned, similarly sized) grains along the line of sight to a background star, and thus that polarization maps are not necessarily simple geometric projections of the interstellar magnetic field (§ 4). We find that elongated cold dark clouds such as B216-217 and L1755, which represent a sharp maximum in the number of *extinguishing* grains along the line of sight, apparently do not represent such a maximum in the distribution of *polarizing* grains. The observed polarization for each star needs to be considered not only as the geometric sum of the effects of all fields along the ine of sight to the star (as has been done by Jones 1989; Jones, Klebe, & Dickey 1992, hereafter JKD; MG), but instead as this sum weighted by a changing polarization efficiency along the line of sight. We conclude that a polarization map of background starlight for any region where such a biased distribution of grain properties exists cannot give an unbiased view of the magnetic field.

2. DATA

As in Paper I, we surveyed the region of interest for suitable background stars using the National Optical Astronomy Observatory (NOAO) near-infrared array camera (IRIM) at Kitt Peak National Observatory (KPNO), and then we measured polarization one star at a time using the Minnesota Infrared Polarimeter (MIRP) on the Infrared Telescope Facility (IRTF).

2.1. *Near-Infrared Imaging to Find Background Sources*

In 1991 July, using the IRIM camera (see Fowler et al. 1987) on the 1.3 m telescope at Kitt Peak, we surveyed the most highly extinguished portions of L1755 by creating 19 abutting mosaicked images, each with a field of view of about 8′ × 8′. Each mosaic represents 64 10-s-long pointings of the camera, which itself contains a 58 × 62 element InSb array. The observing procedure at Kitt Peak was very similar to that described in Lada et al. (1991). All fields were observed using the K(2.2 μm) filter. A total of approximately 900 sources were identified in the K-band mosaics, and the survey is complete to about 13th magnitude at K.

2.2. *Near-Infrared Polarimetry with MIRP*

Background stars were selected from the sources identified in the KPNO survey of L1755 using primarily the criteria that the star be (1) brighter than 12th magnitude at K, (2) significantly reddened in that the star had no, or only a very faint, optical counterpart, (3) located in the region of L1755 which is inaccessible to optical polarimetry (i.e., $A_V \gg 1$).

The polarization observations were carried out in 1992 May and 1993 June at the IRTF, using MIRP (see Jones & Klebe 1988). In each integration, we sought to achieve an error of less than 1 part in 8 in the percentage polarization, which corresponds to an uncertainty in the polarization position angle of less than about 4° (Serkowski 1974). Linear polarization was determined to this accuracy or better, at at least one wavelength, for 53 stars. Polarization was measured for 50 of the 53 stars at J(1.22 μm), 35 at H(1.65 μm), and 31 at K (see Table 1). The relative difficulty of measuring polarization at a particular wavelength depends on two competing trends. Stars polarized by interstellar dust give a larger percentage polarization at the shorter infrared wavelengths, but highly reddened stars are brighter at the longest wavelength. In § 3.2, we discuss the

TABLE 1

JHK POLARIMETRY AND PHOTOMETRY IN L1755

Star #	Right Ascension (1950)			Declination (1950)			p_J	σ_{p_J}	θ_J	σ_{θ_J}	J	p_H	σ_{p_H}	θ_H	σ_{θ_H}	H	p_K	σ_{p_K}	θ_K	σ_{θ_K}	K	"p_K"	$\sigma_{\text{"}p_K\text{"}}$	$\theta_{\text{"}p_K\text{"}}$	$\sigma_{\theta_{\text{"}p_K\text{"}}}$	J-K	A_V
	[h]	[m]	[s]	[deg]	[min]	[sec]	[%]	[%]	[deg]	[deg]	[mag]	[%]	[%]	[deg]	[deg]	[mag]	[%]	[%]	[deg]	[deg]	[mag]	[%]	[%]	[deg]	[deg]	[mag]	[mag]
(1)	(2)	(3)	(4)	(5)	(6)	(7)	(8)	(9)	(10)	(11)	(12)	(13)	(14)	(15)	(16)	(17)	(18)	(19)	(20)	(21)	(22)	(23)	(24)	(25)	(26)	(27)	(28)
1	16	36	13.3	-22	17	31	2.47	0.12	57	1	10.57	1.74	0.14	64	2	9.17	1.21	0.25	56	6	8.81	0.89	0.04	59	1	1.76	4.3
2	16	36	14.0	-22	20	16	2.11	0.16	59	2	10.69	1.43	0.33	55	7	9.47					9.20	0.71	0.05	59	2	1.49	2.7
3	16	36	44.5	-22	14	19	3.47	0.03	55	1	12.09					10.99					10.68	1.16	0.01	55	1	1.41	2.3
4	16	36	48.6	-22	14	53	2.48	0.29	60	3	11.74	2.02	0.62	59	9	10.67	1.71	0.46	61	8	10.45	1.07	0.13	60	3	1.29	1.6
5	16	36	52.4	-22	15	58	2.33	0.40	67	5	12.39					11.10	2.35	0.47	59	6	10.79	1.44	0.21	64	4	1.60	3.4
6	16	37	09.9	-22	17	31	1.16	0.17	75	4	11.87					10.49	0.41	0.13	84	9	10.11	0.40	0.08	76	4	1.76	4.3
7	16	37	18.0	-22	12	33	2.89	0.56	53	6	12.21	1.98	0.19	59	3	10.54					10.04	0.99	0.09	58	3	2.17	6.6
8	16	37	21.0	-22	08	17	4.01	0.21	53	2	11.04	2.35	0.48	52	6	10.31	1.74	0.31	59	5	10.20	1.43	0.10	54	2	0.84	0.0
9	16	37	30.9	-22	14	29	1.44	0.15	49	3	10.89					9.24					8.70	0.48	0.05	49	3	2.19	6.7
10	16	37	31.4	-22	07	58	3.35	0.20	52	2	10.71	1.81	0.25	41	4	9.72	0.83	0.25	54	9	9.51	0.98	0.08	50	2	1.20	1.1
11	16	37	35.4	-22	13	50	2.88	0.83	69	8	12.92					11.37	1.67	0.46	41	8	10.88	1.50	0.36	55	6	2.04	5.8
12	16	37	37.2	-22	15	17	1.59	0.12	71	2	9.46	0.96	0.07	72	2	7.72	0.68	0.07	72	3	7.12	0.57	0.03	72	1	2.34	7.5
13	16	37	57.5	-22	12	59	2.92	0.15	58	2	10.68	1.93	0.11	57	2	9.22	0.74	0.18	62	7	8.84	0.92	0.05	58	1	1.84	4.7
14	16	38	14.6	-22	15	44	0.93	0.05	74	2	8.57					7.19	0.66	0.08	62	3	6.87	0.41	0.03	70	2	1.70	3.9
15	16	38	23.1	-22	13	32	2.79	0.29	43	3	11.31	2.31	0.35	46	4	10.18	1.74	0.23	45	4	9.91	1.37	0.12	44	2	1.40	2.2
16	16	38	38.9	-22	14	06	1.80	0.26	68	4	11.32	0.99	0.19	69	5	10.11					9.87	0.53	0.07	68	3	1.45	2.5
17	16	38	52.3	-22	10	08	2.35	0.28	53	3	12.19					10.97					10.71	0.78	0.09	53	3	1.48	2.7
18	16	39	00.0	-22	06	17	2.89	0.48	43	5	11.99	1.09	0.25	36	7	10.75					10.48	0.63	0.10	40	4	1.51	2.9
19	16	39	15.5	-21	44	35	2.97	0.08	58	1	8.17											0.99	0.03	58	1		
20	16	39	30.2	-21	57	10	2.20	0.24	48	3	11.96	1.91	0.31	27	5	10.9	2.37	0.71	22	9	10.78	0.92	0.09	41	2	1.18	1.0
21	16	39	51.3	-22	01	08	2.56	0.21	69	2	11.66	1.65	0.36	60	6	10.40	0.77	0.10	69	4	10.28	0.79	0.08	68	2	1.38	2.1
22	16	39	58.3	-21	53	37	2.29	0.09	47	1	9.73					8.31					7.96	0.76	0.03	47	1	1.77	4.3
23	16	40	32.0	-21	49	02	1.74	0.29	58	5	11.90					10.29					9.89	0.58	0.10	58	5	2.01	5.7
24	16	40	49.8	-21	49	47	2.53	0.14	67	2	10.54					9.03					8.64	0.84	0.05	67	2	1.90	5.0
25	16	40	55.8	-21	47	33	2.54	0.31	60	4	12.02	1.54	0.28	54	5	10.71					10.33	0.80	0.09	58	3	1.69	3.9
26	16	40	57.0	-21	48	38	1.88	0.58	54	9	12.31					11.15					10.79	0.63	0.19	54	9	1.52	2.9
27	16	41	11.0	-21	40	46	3.02	0.23	57	5	11.71	2.24	0.32	56	5	10.94					10.73	1.05	0.07	57	4	0.98	0.0
28	16	41	22.6	-21	40	15	3.15	0.22	56	5	10.42	1.52	0.21	56	5	8.95	1.06	0.21	54	6	8.50	0.95	0.08	56	3	1.92	5.2
29	16	41	55.6	-21	36	28	3.00	0.11	62	1	9.77	1.58	0.12	60	2	9.19	0.69	0.10	58	4	9.07	0.82	0.04	62	1	0.70	0.0
30	16	41	56.1	-21	32	25	2.48	0.13	51	1	10.38	1.41	0.10	53	2	9.12	1.01	0.05	53	1	8.77	0.94	0.04	52	1	1.61	3.4
31	16	42	15.0	-21	11	06	3.16	0.21	23	2	10.90	3.25	0.86	21	8	10.14	1.26	0.38	25	9	9.67	1.12	0.10	23	2	1.23	1.3
32	16	42	20.0	-21	18	26	0.75	0.14	21	5	10.11					9.71	0.46	0.05	27	3	9.21	0.44	0.04	26	3	0.90	0.0
33	16	42	23.7	-21	34	36	2.70	0.26	62	3	11.37	1.87	0.18	61	3	9.90	1.39	0.26	59	5	9.82	1.04	0.08	61	2	1.55	3.1
34	16	42	24.1	-21	22	23	2.59	0.71	80	8	13.88					13.04					13.38	0.86	0.24	80	8	0.50	0.0
35	16	42	24.6	-21	31	49	3.09	0.10	62	1	9.27	1.78	0.11	61	2	8.01	0.98	0.14	44	4	7.67	0.97	0.04	61	1	1.60	3.4
36	16	42	26.7	-21	23	36					13.47	4.57	1.50	84	9	12.10					11.74	2.29	0.75	84	9	1.73	4.1
37	16	42	29.8	-21	16	31	6.22	1.95	179	9	13.53	1.95	0.29	13	4	11.87					11.22	1.00	0.14	40	4	2.31	7.3
38	16	42	32.1	-21	16	01					13.57					11.93	0.70	0.23	17	10	11.43	0.70	0.23	17	10	2.14	6.4
39	16	42	37.7	-21	17	12	5.25	1.57	68	9	13.93	4.94	0.63	66	4	11.82	1.12	0.28	62	7	11.25	1.35	0.23	65	3	2.68	9.4
40	16	42	38.4	-21	23	03					13.10	2.38	0.53	63	6	11.39					10.84	1.19	0.27	63	6	2.26	7.1
41	16	42	40.0	-21	24	24	2.58	0.38	76	4	12.16	1.97	0.05	60	1	10.62	1.33	0.33	19	7	10.14	0.99	0.03	60	1	2.02	5.7
42	16	42	42.2	-21	35	41	2.51	0.11	58	1	9.89	1.45	0.08	57	2	8.48	1.02	0.10	58	3	8.16	0.84	0.04	58	1	1.73	4.1
43	16	42	42.7	-21	18	51	1.90	0.07	61	1	8.37	1.24	0.20	56	5	6.56	0.90	0.13	66	4	5.92	0.69	0.03	61	1	2.45	8.1
44	16	42	45.7	-21	24	22	3.76	0.69	97	5	12.60	1.32	0.30	84	7	10.95					10.43	0.75	0.13	93	4	2.17	6.6
45	16	42	49.9	-21	09	46	2.33	0.49	41	6	13.06					11.73					11.38	0.78	0.16	41	6	1.68	3.8
46	16	42	52.0	-21	15	46	3.91	0.54	75	4	11.89	2.30	0.28	74	3	10.45	1.14	0.24	73	6	9.97	1.16	0.14	74	2	1.92	5.2
47	16	42	52.5	-21	20	26	2.39	0.08	53	1	9.49	1.36	0.08	49	2	8.13	0.82	0.10	53	3	7.71	0.76	0.03	52	1	1.78	4.4
48	16	43	08.0	-21	13	21	6.08	0.08	51	1	11.44	2.78	0.40	53	4	10.49	2.38	0.22	57	3	10.16	2.04	0.03	52	1	1.28	1.6
49	16	43	14.0	-21	14	29	3.64	0.07	56	1	10.25	2.17	0.28	52	4	8.80	1.30	0.10	56	2	8.38	1.24	0.04	56	1	1.87	4.9
50	16	43	23.0	-21	07	16	3.16	0.39	59	4	12.53					11.22					10.92	1.05	0.13	59	4	1.61	3.4
51	16	43	43.7	-21	08	44	3.85	0.46	51	3	10.44	2.05	0.06	43	1	9.28					9.03	1.03	0.03	43	1	1.41	2.3
52	16	43	46.7	-21	11	50	2.53	0.23	56	3	10.57	1.46	0.11	64	2	9.24	1.27	0.25	44	6	8.87	0.82	0.05	60	2	1.70	3.9
53	16	43	52.0	-21	06	51	1.95	0.15	46	2	10.92						0.68	0.16	40	7	9.43	0.66	0.08	46	2	1.49	2.7

NOTE.—Col. (1) Reference number used in text; (2)–(7) 1950 equatorial coordinates of each star; (8) measured percentage polarization at *J* band; (9) 1 σ error in percentage polarization at *J* band; (10) position angle (east of north) of polarization measured at *J* band; (11) 1 σ error in position angle of polarization measured at *J* band; (12) *J* magnitude in the IRTF/MIRP system; (13)–(17) same as (8)–(12), for *H* band; (18)–(22) same as (8)–(12), for *K* band; (23) "estimated" *K*-band polarization, calculated according to eq. (3); (24) 1 σ error in "estimated" *K*-band polarization, calculated according to eq. (4); (27) difference of cols. (12) and (22); (28) visual extinction, calculated according to eq. (5).

measured wavelength dependence of polarization in L1755, and its origin.

3. RESULTS

3.1. *Polarization Direction and Dispersion*

Maps of the polarization of background starlight in the part of the sky containing the dark cloud L1755, at both optical and near-infrared wavelengths, are exhibited in Figure 1. From the figure, it is clear that the pattern of polarization vectors viewed through the densest regions of the dark cloud using near-infrared polarimetry greatly resembles the pattern of polarized vectors measured through the periphery of the cloud using optical polarimetry. Furthermore, as is apparent upon inspection of Figure 2, the mean direction and dispersion of the near-infrared polarization vectors are very similar to the optically derived direction and dispersion.

To verify the apparent similarity of the distributions shown in Figure 2, the observed distributions of polarization position angle can be modeled as the sum of contributions from a uniform and a nonuniform magnetic field, using the technique

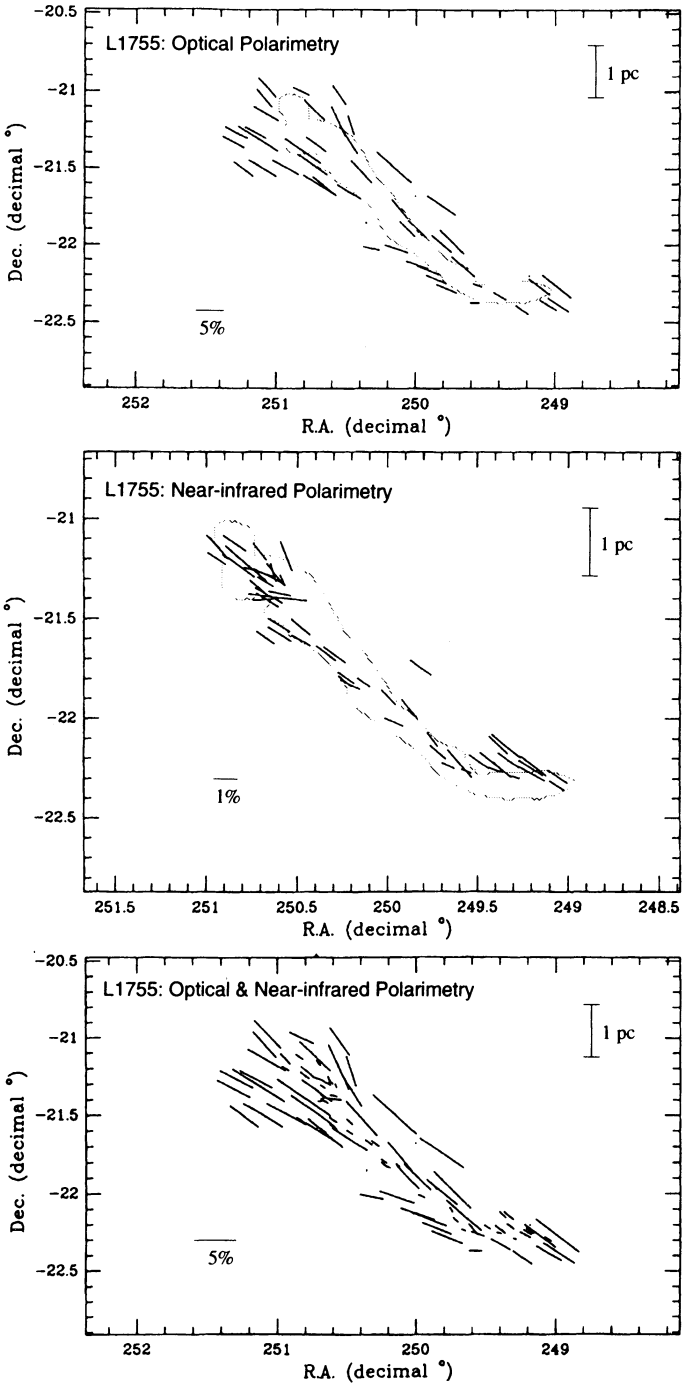

FIG. 1.—*Top panel*, Optical polarization map of the L1755 dark cloud (Goodman et al. 1990); *middle panel*, infrared polarization map of the L1755 dark cloud, based on the data in Table 1; *bottom panel*, superposition of optical and infrared polarimetry based on the data shown in the two panels above. The length of the vectors is proportional to "p_K" for the infrared data, and $p_{6500\,A}$ for the optical data, with the scale as indicated, in all panels. A single contour in the upper two panels shows the extent of the L1755 dark cloud, as traced by the $T_R^* = 3$ K contour of ^{13}CO (Loren 1989).

described by MG, which is similar to the method first proposed by Chandrasekhar & Fermi (1953). The fits using this technique are shown in Figure 2, and they give mean position angles for the optical and infrared polarization data which are within one standard deviation of each other: 59° ± 1° for the optical data and 57° ± 1° for the near-infrared data. In the context of the MG model, the width (dispersion) of an observed distribution of polarization position angle is related to the parameter *s*, which is equal to the ratio of the non-uniform to the uniform field strength, divided by the square root of the number of field correlation lengths along the line of sight (see Paper I and MG). In cases where the distribution of polarization position angle is roughly Gaussian, as is the case in L1755, *s* is equal to the 1 σ dispersion of a Gaussian fit to the distribution, expressed in radians. The derived values of *s* are very similar for the optical and near infrared data in L1755: 0.22 ± 0.01 and 0.17 ± 0.01 radians, respectively. In fact, only in the small region near ($\alpha_{1950} = 250\overset{\circ}{.}70$, $\delta_{1950} = -21\overset{\circ}{.}35$) does the infrared polarimetry direction and dispersion differ from the pattern one would extrapolate from optical polarimetry. The situation in L1755 is very similar to what was encountered in B216-217 in Paper I: there is, for the most part, no difference in polarization direction and dispersion when comparing regions "inside" and "outside" of a dark cloud, in projection. This detailed similarity between optical and near-infrared polarization in dark clouds is also evident in observations of Taurus (Tamura et al. 1987), Ophiuchus (Wilking et al. 1979), and Perseus (Tamura et al. 1988).

3.2. *Wavelength Dependence of Polarization*

The wavelength dependence of polarization is a good diagnostic of the size distribution of polarizing grains along a line of sight since the amount of polarization of background starlight produced at any particular wavelength depends strongly on the ratio of grain size to wavelength (see Fig. 3). The details of the processes conspiring to produce the observed wavelength dependence of polarization are not very well understood (see Whittet 1995); they are discussed in § 4.2.1.

3.2.1. *Serkowski Relation*

Empirically, it has been shown that the wavelength dependence of polarization in the ultraviolet to near-infrared wavelength range is well approximated by the relation of the form

$$\frac{p}{p_{\max}} = \exp\left[-K \ln^2\left(\frac{\lambda_{\max}}{\lambda}\right)\right]. \quad (1)$$

Serkowski (e.g., Serkowski et al. 1975) was the first to write down this relation, which now often bears his name. In his formulation, K is constant, with a value ≈ 1.15. Wilking et al. (1980; Wilking, Lebofsky, & Rieke 1982) measured the wavelength dependence of the polarization of background starlight in the near-infrared, and by combining their results with existing optical data, they find a correlation between K and $\lambda_{\max}$ of the form

$$K = (-0.10 \pm 0.05) + (1.86 \pm 0.09)\lambda_{\max}, \quad (2a)$$

where $\lambda_{\max}$ is expressed in microns. Whittet et al. (1992) have recently carried out a wavelength-dependence investigation similar to those of Wilking et al. (1980, 1982), with wavelength coverage into the near-infrared, and they find a relation very similar to the Wilking et al. results:

$$K = (0.01 \pm 0.05) + (1.66 \pm 0.09)\lambda_{\max}. \quad (2b)$$

Regardless of the exact value of K, the most fundamental features of equation (1) are clear. The observed percentage polarization of a background star increases monotonically with increasing wavelength until it peaks at a percentage $p_{\max}$ at the wavelength $\lambda_{\max}$, and then the percentage decreases

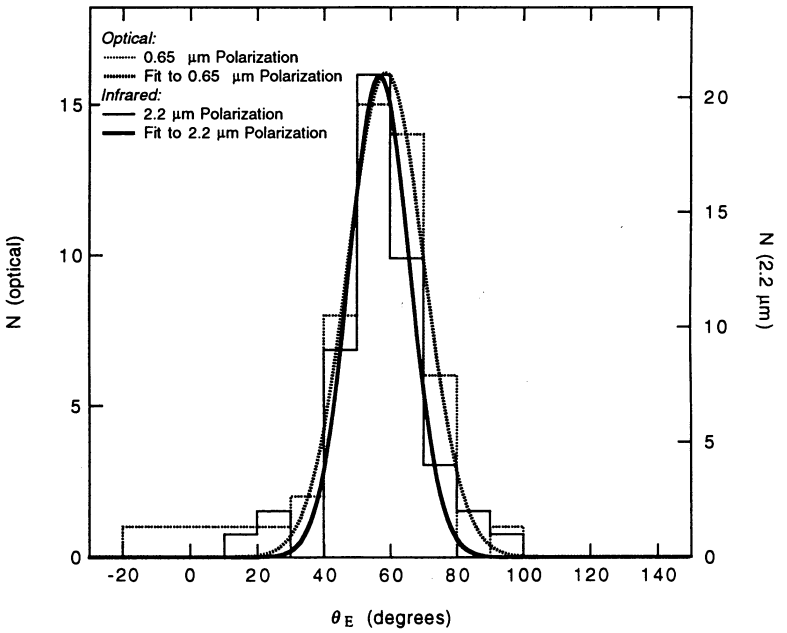

FIG. 2.—Dispersion in polarization position angle in dark cloud L1755. Fits of the MG model (shown as smooth curves) described in § 3.1 give mean position angles for the optical (Goodman et al. 1990) and infrared polarization data which are within one standard deviation of each other: 59° ± 1° for the optical data and 57° ± 1° for the near-infrared data. The derived values of s (dispersion) are also very similar for the optical and near-infrared data in L1755: 0.22 ± 0.01 and 0.17 ± 0.01 radians, respectively.

monotonically as the wavelength is increased. The value of λ_{max} is closely related to the size of a "typical" polarizing grain along a line of sight.

3.2.2. *Use of the Serkowski Relation on JHK Data Alone*

When the polarization of a star's radiation has been measured at numerous wavelengths, it is straightforward to fit the function given in equations (1) and (2) to the $p(\lambda)$ data in order to determine K, p_{max}, and λ_{max} (e.g., Wilking et al. 1980, 1982; Whittet et al. 1992). Normally, this procedure is not carried out for JHK polarization data on its own, for three reasons. First, the near-infrared wavelengths spanned by the JHK filters almost always lie on one side of the wavelength of peak polarization (λ_{max}), so one is heavily reliant on the exact functional form of equation (1) in determining K, p_{max}, and λ_{max}. Second, it is hard to assess goodness of fit when fitting a function with three free parameters (eq. [1]) to three measured quantities (the polarizations at J, H, and K). And, third, there is so little variation in the ratios between polarizations measured at J, H, and K (as compared with shorter wavelengths) that there have been proposals of an empirical "universal polarization law" in the near-infrared, which takes the form of a simple power law (e.g., Martin & Whittet 1990). If such a universal power law were to actually exist, it would not be possible to predict λ_{max} from JHK polarization data alone (although the normalization of this power law would presumably be related to p_{max}).

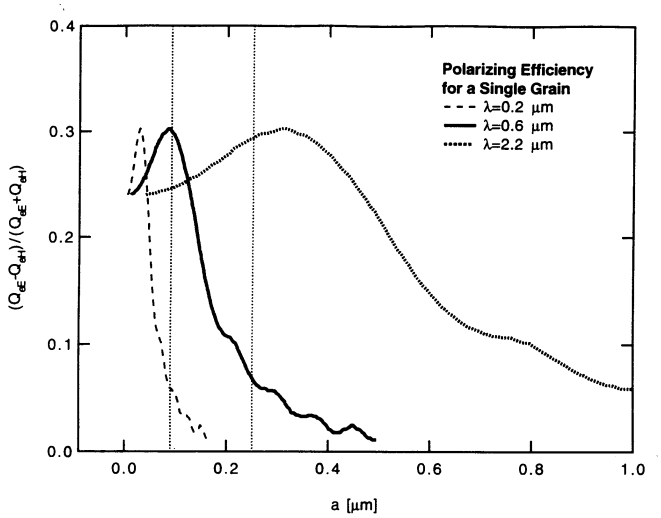

FIG. 3.—Theoretical estimates of the ratio of polarization to extinction for a single prolate grain with 20% porosity and 2:1 aspect ratio, as a function of semiminor axis length, a (based on Wolff et al. 1994). The theoretical curves show $(Q_{eE} - Q_{eH})/(Q_{eE} + Q_{eH})$, where Q_{eE} and Q_{eH} are the extinction efficiency factors for a grain whose long axis is parallel to either the electric or magnetic vector, respectively, of the incident radiation. For these curves, the direction of propagation is assumed to be perpendicular to the long axis of the grain, and the effective index of refraction is calculated using a discrete-dipole approximation (DDA).

Despite these limitations, we have managed to fit the Serkowski relation (eq. [1]) to JHK polarization data alone with demonstrable success. Before fitting our L1755 data, we tested our fitting algorithm on the $UBVRIJHK$ polarization data sets for the Chamaeleon and R CrA dark clouds presented in Whittet et al. (1992). When the polarization data for all eight wavelengths are used, our nonlinear weighted least-squares fitting routine confirms the values of K, p_{max}, and λ_{max} found by Whittet et al. exactly. When we use *only the* JHK data points from Whittet et al., the results are surprisingly good: typically, λ_{max} differs from the fit using all of the $UBVRIJHK$ data by less than 0.1 μm, p_{max} will be off by less than one-tenth of its value, and K will be off by less than 0.1.

In cases where only J, H, and K polarization data are available and one has no a priori knowledge of K, p_{max}, or λ_{max}, fitting equation (1) with three free parameters prohibits proper error estimation. So, in order to allow for reliable error esti-

mates, one can allow K to depend on λ_{max} as in equation (2a) or (2b), so that just two free parameters (λ_{max} and p_{max}) are fit to three data points. Again using the Whittet et al. data as a test case, we find that, typically, the rms differences between a two-parameter fit to *JHK* data alone and a three-parameter fit to all eight wavelengths are of order 0.13 μm in λ_{max} and $0.14p_{max}$ in p_{max}. Furthermore, the two-parameter fits return 1 σ errors which are equivalent to these rms differences. Thus, we except that fitting equation (1) with K constrained by equation (2b) is a reasonably reliable technique for estimating λ_{max} and p_{max} from high-quality *JHK* polarimetry, insofar as the Serkowski relation is representative of the wavelength dependence of polarization in the near-infrared.

There are 24 stars in our L1755 sample where we have measured polarization at *J*, *H*, and *K*. The results of applying the two-parameter fitting procedure described above to those data produced the values of λ_{max} and p_{max} listed in Table 2. The 1 σ errors listed in Table 2 are for fits where the weights are proportional to $1/\sigma_{p_i}^2$, where σ_{p_i} is the measurement uncertainty in the polarization at band *i*. The weights are normalized so that χ^2 is equal to the number of data points. Figure 4 presents four sample fits to stars with λ_{max} value ranging from 0.40 to 1.35 μm. For all but one star (No. 41) in Table 2, the position angle of polarization is independent of wavelength, as it should be when polarization is caused by dust along an extended line of sight. In three cases, the fitting is so poor (stars 10, 29, and 39) that it cannot be considered at all reliable. So, in the analysis of the distributions of λ_{max} and p_{max} discussed in the next section, we do not include stars 41, 10, 29, and 39.

3.2.3. *Large Range of λ_{max} near L1755*

The values of λ_{max} and p_{max} derived from the *JHK* polarimetry in L1755 are displayed graphically in Figure 5. If λ_{max} and p_{max} were truly independent parameters, there should be no correlation evident in the plot of λ_{max} versus p_{max}. Given that some correlation is evident, and that we have fixed λ_{max} to depend on K in equation (1) by using equation (2b), the implication is that at least two of the three parameters (λ_{max}, p_{max}, and K) used in the Whittet et al./Wilking et al. formulation of the Serkowski relation are correlated—and perhaps all three. This lack of independence among parameters calls into question the applicability of this functional form. Without data at shorter wavelengths, we have no way to "prove" that the Serkowski relation described in equations (1) and (2b) applies in L1755. For lack of a good reason to believe that it does not apply, we will make the (conventional) assumption that the

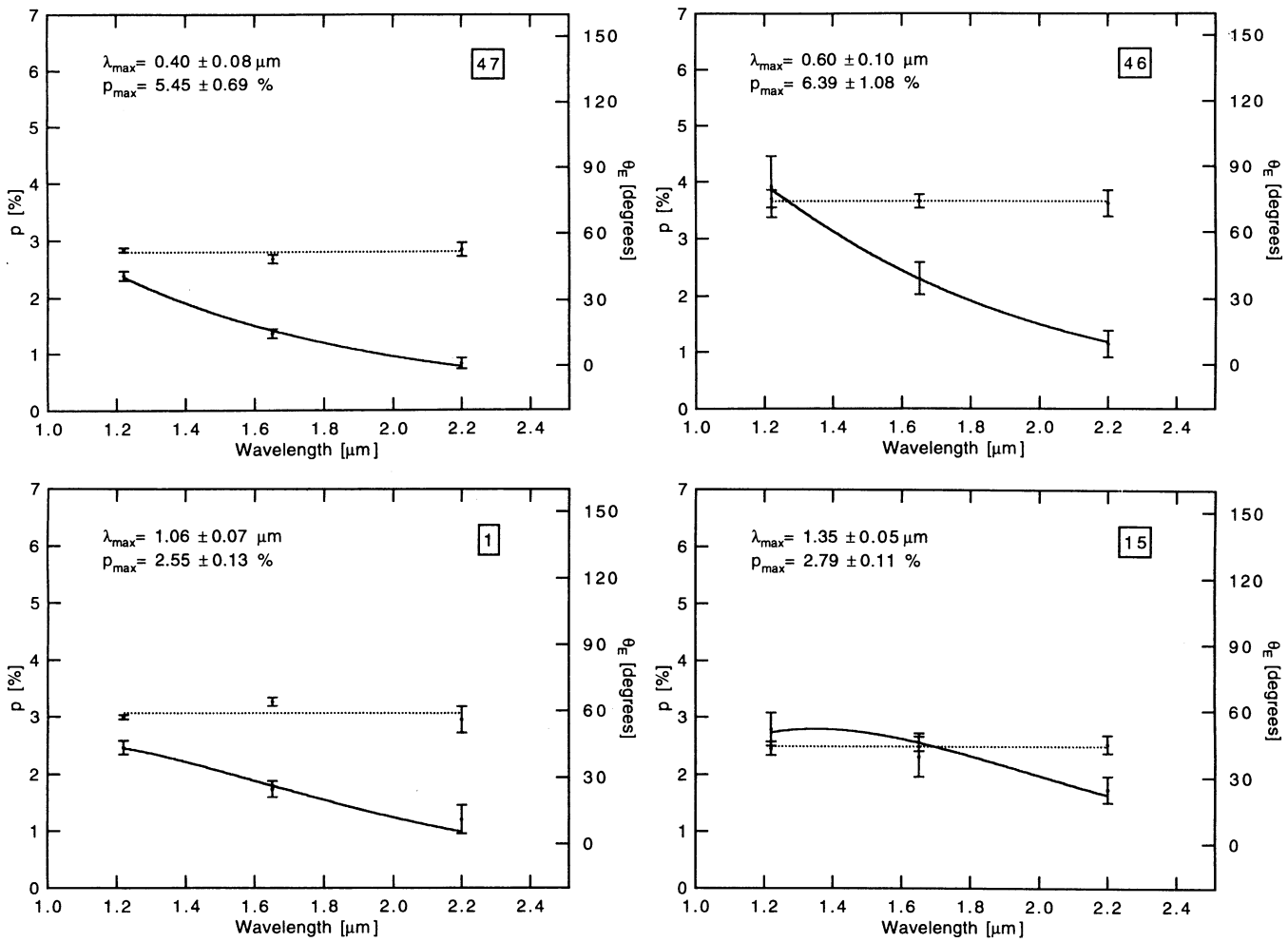

FIG. 4.—Sample fits (*solid lines*) of a Serkowski relation (eq. [1]) with $K = 0.01 + 1.66\lambda_{max}$ for stars in L1755. The plots are arranged showing a progression of increasing λ_{max}, beginning with the upper left panel. Boxed labels refer to the star numbers in Tables 1 and 2, and the fit values are derived as described in § 3.2. Dashed lines show linear fits to position angle as a function of wavelength.

TABLE 2

WAVELENGTH DEPENDENCE OF POLARIZATION IN L1755

Star Number	λ_{max} (μm)	$\sigma_{\lambda_{max}}$ (μm)	p_{max}	$\sigma_{p_{max}}$	Notes
1.....	1.06	0.07	2.55%	0.13%	
4.....	1.38	0.07	2.54	0.10	
8.....	1.00	0.12	4.26	0.39	
10	0.56	0.65	5.78	6.08	1, 2
12	0.97	0.17	1.66	0.33	
13	0.83	0.12	3.62	0.57	
15	1.35	0.05	2.79	0.11	
20	1.40	0.15	2.25	0.18	
21	0.68	0.10	3.75	0.54	
28	0.46	0.38	6.31	3.92	
29	0.57	0.88	4.99	7.06	1, 2
30	1.04	0.14	2.47	0.42	
31	1.15	0.11	3.20	0.16	
33	1.10	0.11	2.68	0.27	
35	0.47	0.07	6.28	0.72	
39	0.72	1.72	7.72	21.35	1, 2
41	1.15	0.07	2.52	0.16	2, 3
42	0.76	0.24	3.30	1.12	
43	1.11	0.08	1.93	0.08	
46	0.60	0.10	6.39	1.08	
47	0.40	0.08	5.45	0.69	
48	0.74	0.38	8.29	4.01	
49	0.90	0.05	4.17	0.20	
52	0.24	0.12	7.07	0.59	

NOTES.—(1) Very poor fit, error exceeds value; (2) excluded from Fig. 5; (3) position angle varies with wavelength.

λ_{max} derived by fitting the Serkowski relation is a legitimate diagnostic of the typical grain size along a line of sight.

The histograms in Figure 5 show that both p_{max} and λ_{max} have large average values and large dispersions in L1755. The p_{max} distribution is difficult to interpret in an unambiguous way since the absolute value of percentage polarization can be affected by several properties other than grain size (see Table 4), and we will not discuss it further. The large average (0.88 μm) and standard deviation (0.34 μm) of λ_{max} evident in Figure 5 is striking and implies a large range of grain properties along the lines of sight observed. The width of this distribution is broadened to some extent by the relatively large errors ($\sim$0.13 μm) inherent in estimating λ_{max} from J, H, K data alone (§ 3.2.2), but even after correcting for this effect, the standard deviation of the distribution is 0.31 μm, which means that the 1 σ range in λ_{max} spans a factor of 2 (from 0.6 to 1.2 μm) in L1755. For comparison, note that Whittet et al. (1992) find a range of $0.3 < \lambda_{max} < 0.9$ μm for dark-cloud lines of sight in general, and a factor-of-2 variation within a region the size of L1755 is not atypical. The nearest cloud to L1755 in Whittet et al.'s sample is ρ Oph, where the typical λ_{max} is $\sim$0.72 μm.

We have checked for any correlation between λ_{max} and extinction in L1755, and we find none. Such correlations have been found in other regions of Ophiuchus (Vrba, Coyne, & Tapia 1993) and have been used as evidence for larger grains being associated with denser gas. The fact that we see no such correlation supports the idea (see § 4) that the grains producing the polarization observed are not associated with the dense interior of L1755.

There are two key implications of a large range of λ_{max} within localized regions of the ISM. First, it makes estimation of polarization measured at one wavelength based on data at only one other wavelength quite an inexact process (§ 3.2.4). Second, it means that the polarizing grains along neighboring lines of sight can vary significantly in their properties, and that we must consider the ramifications of this variation carefully.

3.2.4. *Calculating K-Band Polarization for Comparisons with Earlier Work*

Even though the analysis above shows that it is not possible to accurately estimate polarization at one wavelength from a measurement at another wavelength without an a priori knowledge of λ_{max}, such estimates are routinely made by assuming a "canonical ISM" value for λ_{max}. In Paper I, we did just this by calculating "p_K" and "σ_{p_K}" (listed without quotes in Table 1 of Paper I) using the following definitions, with the measured polarizations and their errors represented by p_J, p_H, p_K, σ_{p_J}, σ_{p_H}, and σ_{p_K}, respectively:

$$\text{“}p_K\text{”} = \left(\frac{p_K}{\sigma_{p_K}^2} + \frac{p_H}{2\sigma_{p_H}^2} + \frac{p_J}{3\sigma_{p_J}^2}\right)\left(\frac{1}{\sigma_{p_K}^2} + \frac{1}{\sigma_{p_H}^2} + \frac{1}{\sigma_{p_J}^2}\right)^{-1}, \quad (3)$$

$$\text{“}\sigma_{p_K}\text{”} = \sqrt{\left(\frac{1}{\sigma_{p_K}}\right)^2 + \left(\frac{1}{2\sigma_{p_H}}\right)^2 + \left(\frac{1}{3\sigma_{p_J}}\right)^2}\left(\frac{1}{\sigma_{p_K}^2} + \frac{1}{\sigma_{p_H}^2} + \frac{1}{\sigma_{p_J}^2}\right)^{-1}. \quad (4)$$

These definitions follow from the Serkowski relation (eq. [1]) for $\lambda_{max} \approx 0.68$ μm and $K = 1.15$. In this paper, we have used equations (3) and (4) to calculate the values for "p_K" and "σ_{p_K}" shown in Table 1. It is apparent from Table 1 that the relationship "p_K" $\approx p_K$ is *not satisfied* in most cases where the direct comparison between "expected" and observed K-band polarization is possible. This fact reinforces the idea that there is a large range in grain properties (λ_{max}) in the L1755 region (see § 3.2.3). We only calculate "p_K" in this paper to allow for the direct comparison of the results presented here with results in the literature which are often scaled from other near-infrared wavelengths using equation (1) (e.g., Klebe & Jones 1990). The value of "p_K" is not a very accurate estimator of the true polarization observed at K.

3.3. *Polarization as a Function of Extinction*

The relationship between polarization and extinction provides information about the polarizing effectiveness of grains along the line of sight, and/or about the orientation and structure of the magnetic field. Section 4, below, includes a discussion and a long list (Table 4) of the factors determining the percentage of polarization observed for a given amount of extinction. In this section, we attempt to stick to facts: speculation about whether we can ever completely disentangle the relationship between polarization and extinction is left for § 4 and future work.

3.3.1. *L1755*

Figure 6 shows the polarization of J-band background starlight as a function of $J-K$ color for all of the stars in the vicinity of L1755, where these two quantities were directly measured in our IRTF-MIRP observations. If we assume (see § 3.3.3), that most of the stars in our have an intrinsic $J-K$ color of order 1 mag, then Figure 6 can be easily interpreted as a plot of polarization as a function of extinction. The top axis in Figure 6 shows an estimate of the visual extinction corresponding to the measured color excess, based on equation (5) (see § 3.3.3, below). An unweighted linear least-squares fit to the data in Figure 6 gives $p_J = (0.2 \pm 0.4)(J-K) + (2.4 \pm 0.6)$, where polarization is measured in percent and $J-K$ in magni-

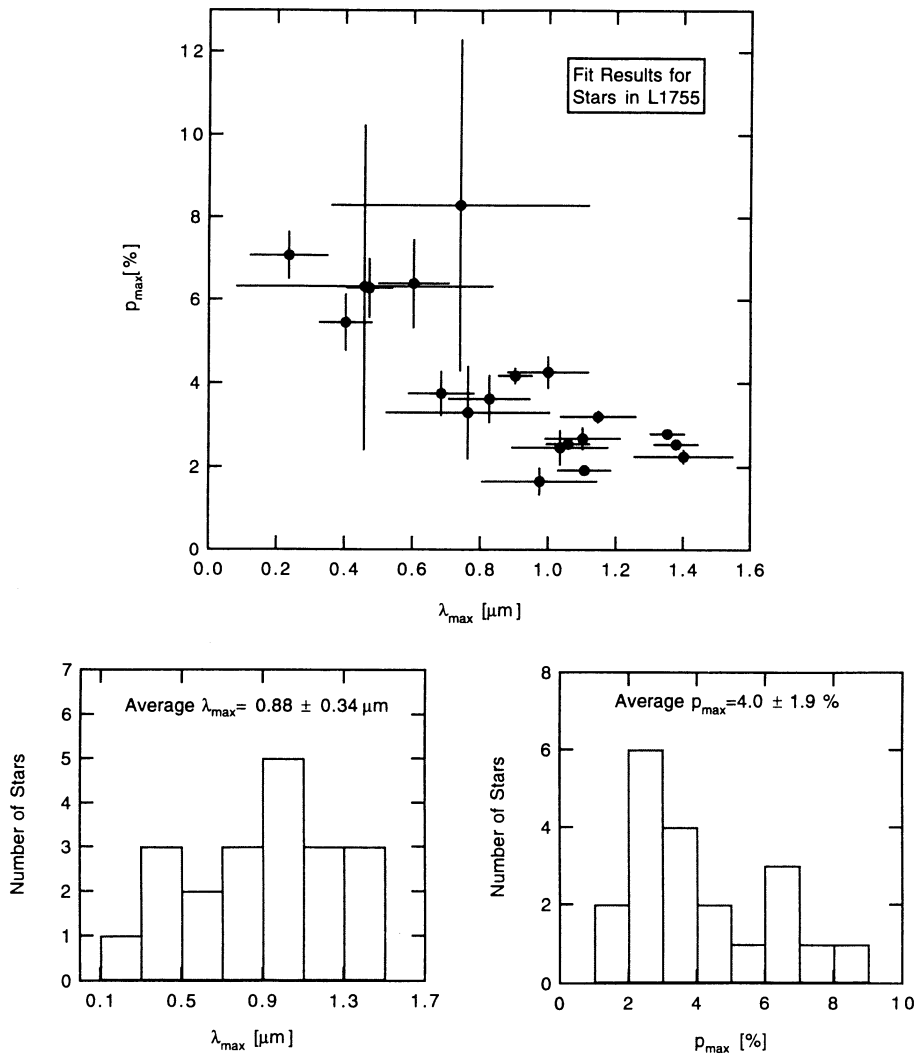

FIG. 5.—λ_{max} and p_{max} in L1755. The correlation evident in the top panel illustrates the lack of independence among the parameters in eq. (1) (see § 3.2.3). The distributions in the two lower panels point out the large ranges and average values of λ_{max} and p_{max} in L1755. The labels show an unweighted mean and standard deviation for each distribution.

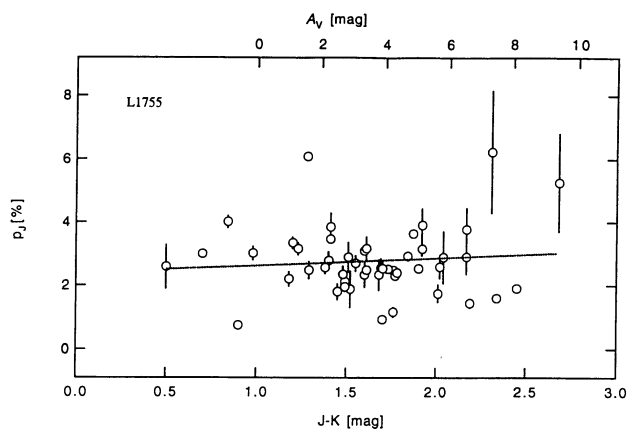

FIG. 6.—Data points show observed percentage polarization at *J* band, as a function of observed $J-K$ color for background stars seen "through" L1755. The top axis shows A_V, calculated using eq. (5). The dotted line shows a fit to these data, which gives $p_J = (0.2 \pm 0.4)(J-K) + (2.4 \pm 0.6)$, where polarization is measured in percent and $J-K$ in magnitudes. The figure clearly shows that polarization does not increase significantly with increasing extinction in L1755.

tudes. This result is consistent with a slope of zero in the polarization-extinction relation, meaning that the "darkest" regions of L1755 are not associated with any more polarization than the lower extinction lines of sight.

3.3.2. *Trends in "Filamentary" and "Round" Dark Clouds*

Figure 7 shows observed relationships between polarization and extinction in most of the dark clouds where polarization of background starlight has now been mapped in the near-infrared.[6] The top panel shows "p_K" versus A_V for L1755 alone, and the middle panel shows the L1755 and B216-217 (Paper I) data sets together. L1755 and B216-217 are the only two highly elongated (i.e., filamentary) cold dark clouds where near-infrared polarimetry is now available. The lower

[6] Bok globules, which ordinarily have masses an order of magnitude below a typical dark cloud, are not included in Fig. 7, but we should note that the inferred polarization efficiency in Bok globules is a factor of 2 lower than that in the general ISM (Klebe & Jones 1990). Small maps of outflow regions are also not included in Fig. 7, since they do not each contain very many data points and extinction measurements are usually not available.

panel shows polarization-extinction relations for three dark clouds which are all closer to round in projection (i.e., bloblike) than L1755 and B216-217 (see references in Fig. 7).

Table 3 presents least-squares linear fits to the data shown in the three panels of Figure 7. The category designations "filamentary" and "round" are meant to distinguish elongated, large, cold, dark clouds like B216-217 and L1755 from denser, smaller, more bloblike, possibly warmer clouds like NGC 1333, HCl 2, and the core of Ophiuchus (L1688). Note that all three panels show K-band polarization on the y-axis, and that equation (3) has been used to convert polarization measured at J, H, and/or K band to "p_K" for the B216-217 and L1755 data.

Straight-line fits to the polarization-extinction relations shown in Figure 7 facilitate comparisons with previous work, but the statistics of the fits (see Table 3) indicate that a straight line is not a good model for the data. In fact, in order to achieve a weighted fit with $\chi_\nu^2 \approx 1$, it is necessary to scale up the 1 σ error bars shown in Figure 7 by large factors (of order the number of points in each fit). For this reason, the unweighted fits are perhaps more reliable than the weighted ones. Regardless, though, of any fit details, the result from Figure 7 is very clear: *either a weighted, unweighted, or by-eye fit to the filamentary dark cloud data implies that polarization does not increase—at all—with extinction in these regions.* The slopes are even slightly negative in some of the fits.

For the bloblike dark clouds shown in the bottom panel of Figure 7, there are many background stars with very high

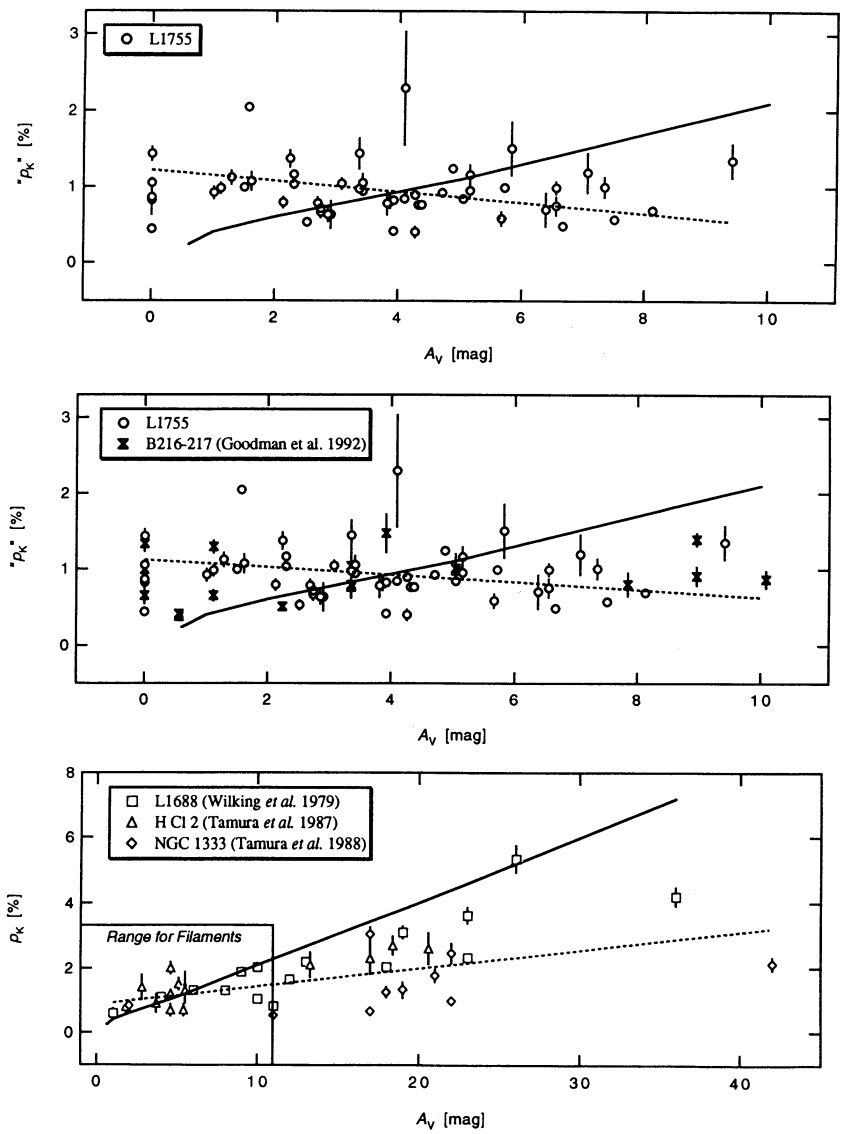

FIG. 7.—Observed relationships between polarization and extinction in dark clouds. *Top panel*, L1755 (this paper); *middle panel*, data for filamentary dark clouds, L1755 and B216-217 (Paper I); *bottom panel*, data for L1688 (Wilking et al. 1979), HCl 2 (Tamura et al. 1987), and NCG 1333 (Tamura et al. 1988), dark clouds which are closer to round, in projection, than L1755 and B216-217 and produce higher extinction. The box in the bottom panel shows how small the range of polarization-extinction space covered by the "filamentary" clouds in the middle panel is in comparison with the range for "round" clouds. All three panels show K-band polarization on the y-axis. Eq. (3) has been used to convert polarization measured at J, H, and/or K band to "p_K" for the B216-217 and L1755 data. *Dashed lines* in each panel show error-weighted least-squares linear fits to the data points (see Table 3). *Solid lines* show the predictions of the JKD model, assuming equal nonuniform and uniform magnetic field energy.

TABLE 3

LEAST-SQUARES FITS TO $p_K = eA_V + p_0$

Cloud and fit	e (% mag^{-1})	σ_e (% mag^{-1})	p_0	σ_{p_0}
L1755 alone:				
Unweighted.....	−0.01	0.02	0.99%	0.10%
Weighted.....	−0.07	0.02	1.21	0.08
Filaments: L1755 and B216-217:				
Unweighted.....	0.00	0.02	0.92	0.07
Weighted.....	−0.05	0.02	1.12	0.07
Blobs: HCl 2, L1688, and NGC 1333:				
Unweighted.....	0.07	0.01	0.82	0.22
Weighted.....	0.06	0.01	0.87	0.13

NOTES.—p_K = "p_K" for L1755 and B216-217. For HCl 2, L1688, and NGC 1333, p_K is equal to the reported value of K-band polarization reported in the references listed in Fig. 3. σ_e and σ_{p_0} denote the 1 σ uncertainties in the fits.

values of visual extinction (tens of magnitudes) available. As a result, the range of extinction covered by the polarization-extinction relation for the bloblike clouds is much larger than for the filamentary clouds, and it is easier to detect a small systematic dependence of p on A_V since the intrinsic measurement error in p is approximately independent of A_V. The slope (listed in Table 3) for the bloblike clouds is significantly greater than zero, but it is still quite small (see § 4.1).

The solid lines in Figure 7, which show models of the p_K-A_V relation proposed by Jones (1989) and JKD, are discussed in § 4.1.2.

3.3.3. *Determination of A_V*

For the three "round" clouds included in Figure 7, the values of A_V were taken directly from the original references. For the B216-217 and L1755 data, visual extinction has been estimated using the relation

$$A_V = rE_{J-K} = 5.6E_{J-K} = 5.6[(J-K) - 1] , \quad (5)$$

where E_{J-K} represents the $J-K$ color excess due to reddening by interstellar dust, and J and K represent, respectively, the J and K magnitudes observed. This relation assumes that the intrinsic $J-K$ color of the background stars we observe is 1 mag because star count models (e.g., Garwood & Jones 1987) imply that most of the background stars included in polarization maps of nearby dark clouds should be K through M giants, which have an intrinsic $J-K$ color of about 1 mag. This assumption introduces typical errors of order ± 1 mag in our estimates of extinction. However, another assumption implicit in equation (5) is that the ratio, r, between visual extinction and $J-K$ color excess is constant along different lines of sight in the ISM. In fact, r varies very significantly along different lines of sight (see Whittet 1992) and only has a mean of ~ 5.6. For example, Whittet's (1992) empirical results that a change in λ_{max} from 0.5 to 1.0 μm will cause approximately a 20% increase in r, and in turn in the value of A_V that one would calculate by using equation (5).[7] In L1755, we know from the results of § 3.2 that such changes in λ_{max} are common, and therefore that the values of A_V calculated using equation (5) with a constant value of r are only good to no better than about 20%. We note, however, that $J-K$ color excess is actually a good indicator of true column density since extinction laws are quite invariant in the infrared (see Mathis 1990, and references therein), and it is only the numerical value of A_V which is affected by variations in r.

[7] The implications of these variations, and their origins, are discussed further by Dickman (1988), Whittet (1992), and Goodman (1995).

We can only derive λ_{max} in L1755 (see § 3.2) for the stars where polarization has been measured at all three near-infrared bands, J, H, and K. So, if we were to require a customized estimate of r based on knowledge of λ_{max} for each star, we would not have as many data points in the top panel of Figure 7 as if we assume an average, constant, value of $r = 5.6$. For this reason, and because we do not know λ_{max} for the B216-217 data points, we have chosen to use equation (5) to estimate A_V in the top two panels of Figure 7.

Happily, since the fits in Table 3 indicate that polarization is independent of extinction ("p_K" $\propto \tilde{A_V}^0$) in B216-217 and in L1755, the assumptions we have used in our estimates of A_V will not affect our conclusions: we can randomly shuffle the points around the x-axis in the polarization-extinction plots for the filamentary dark clouds in Figure 7, but it would still be the case that "p_K" $\propto \tilde{A_V}^0$!

In defense of our simple technique, though, we note that the values of A_V derived using equation (5) imply a spatial distribution of extinction which agrees with Loren's (1989) map of ^{13}CO emission, which has been shown to be a reliable tracer of dense ($n \sim 10^3$ cm^{-3}) gas. Also, for more than 90% of the stars in our sample, the relationship between $J-H$ and $H-K$ color (Fig. 8) is consistent with reddening of K and M giants by interstellar dust.

4. DISCUSSION

4.1. *Interpretation of the p-A_V Relationships*

In Paper I, we presented three possible explanations for the dark cloud's lack of an effect on the observed polarization of background starlight. Either (1) the projected direction of the

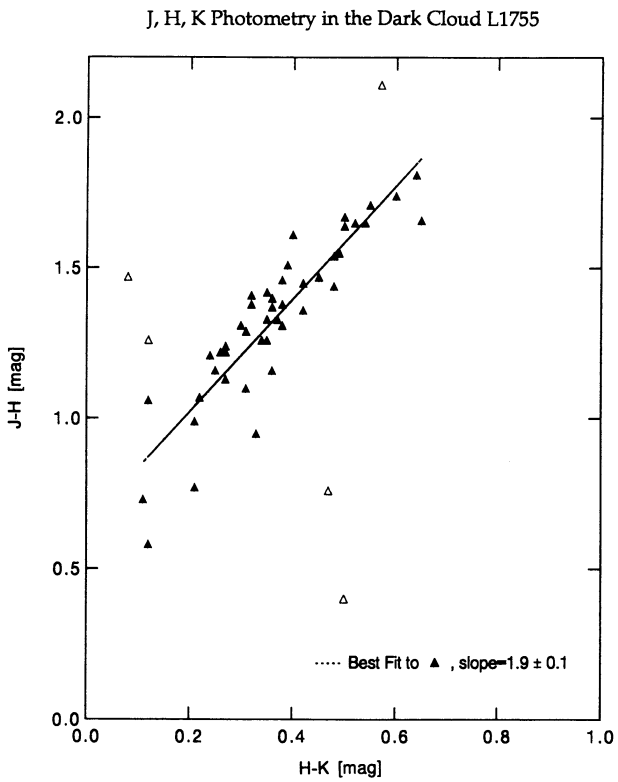

FIG. 8.—JHK color-color diagram. The least-squares fit to the stars shown as solid triangles has a slope consistent with reddening by interstellar dust. The remaining stars (*open triangles*) exhibit either anomalous reddening or poor photometry, but they constitute less than 10% of the total sample.

uniform magnetic field is unaffected by the presence of a dark cloud, (2) the number of field correlation lengths along each line of sight varies in exact proportion to the square of the ratio of nonuniform to uniform field energy, which preserves s (see § 3.1), or (3) polarization of background starlight is not a good tracer of the magnetic field in the dense interiors of dark clouds. The best discriminator between these possibilities is the measured dependence of the percentage polarization on extinction. In scenarios 1 and 2, an increase of percentage polarization with extinction is expected. In B216-217 (Paper I), we found virtually no increase in percentage polarization with increasing extinction, and we favored the third explanation above, concluding that the grains which produce the large extinctions associated with lines of sight through dark clouds are not producing much polarization. In L1755, we also find no increase in polarization with extinction (§ 3.3), which leads us to favor scenario 3 even more strongly than before.

In the next two sections we discuss the implications of the p-A_V relation in the Milky Way as a whole (§ 4.1.1) and in dark clouds in particular (§ 4.1.2).

4.1.1. p-A_V *in the Milky Way's ISM*

For a given number of grains along any line of sight, there is a maximum polarization possible, which would be observed in the case where (1) each grain polarized light equally well and (2) the field were perfectly straight and oriented perpendicular to the line of sight. *The assumption that each grain along a line of sight polarizes equally well is often implicitly accepted, but it is not generally satisfied* (see Wolff et al. 1994; Kim & Martin 1994). The second assumption incorporates the idea that changes in field orientation, due either to changes in the inclination of a uniform field or to field tangling (increase in field nonuniformity), will also reduce the amount of polarization observed for a given amount of extinction (see Jones 1989; JKD).

Figure 9 shows polarization as a function of extinction, observed at visual wavelengths, for 5135 background stars located along random lines of sight in the Milky Way's ISM. It is clear from Figure 9 that there is an upper bound to the amount of polarization possible for a particular extinction, but it is also clear that it is likely that one will observe *any value below* that upper bound. Hiltner, in his 1956 paper which contains a survey of hundreds of stars near the plane of the Milky Way, notes that a correlation between p and A_V is not generally present, but that an upper bound like the one in Figure 9 is prevalent.

At low levels of extinction ($A_V < 2$ mag), it is possible to explain the distribution of data points in Figure 9 with simple geometric arguments—fields perpendicular to the line of sight give the empirically determined "maximum" polarization, $p = 3.0A_V$, while fields with larger inclinations to the plane of the sky give smaller values of p, including $p = 0$ when the field lies exactly along the line of sight. This interpretation is, however, not the whole story. As Hiltner (1956) realized, one can also fill in all of the parameter space below a (fuzzy) upper limit in a p-A_V plane like the one in Figure 9 by allowing the polarizing efficiency of the grains along one line of sight to vary with respect to another line of sight, regardless of field orientation. Hiltner suggested variation in grain alignment efficiency as the main cause of variations in polarizing efficiency. In fact, however, variations in the mean grain size or shape, which cause variations in the wavelength of maximum polarization, λ_{max}, can also cause significant point-to-point variations in polarization efficiency. Significant variations in λ_{max} *are* in fact observed in the ISM (see § 3.2), and they are also theoretically predicted in models which consider realistic grain distributions (e.g., Figs. 7–9 of Wolff et al. 1994).

At larger extinctions, none of the points in Figure 9 lie even close to the $p = 3.0A_V$ line, so something other than changes in the orientation of a *uniform* field must be responsible for the diminished polarization. As noted above, Jones (1989) and JKD have pointed out that field tangling (small-scale changes in the field direction as opposed to a complete reorientation of the uniform field) reduces the value of p for a given A_V.

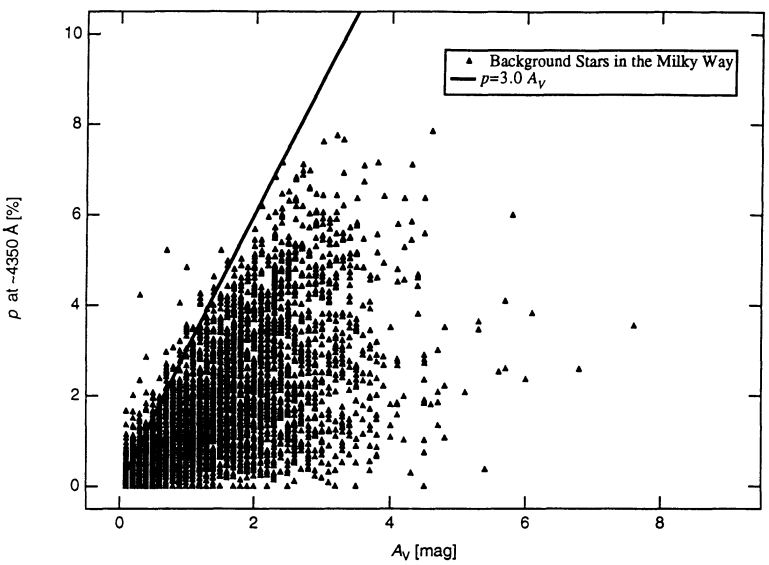

FIG. 9.—$p_{4350\,Å}$ as a function of A_V for 5135 stars seen along random lines of sight through the Milky Way's ISM. Data points are for background stars in the catalog compiled by Mathewson, Ford, & Krautter (1978) and were provided on-line by the NSSDCA. The *solid line* represents the empirical relationship purported to represent the maximum observable percentage polarization for a given amount of extinction $p_V = 3A_V$. Note the trend for most of the parameter space below this line to be filled in at low values of A_V but not necessarily at higher values.

Assuming a single type of polarizing grain, of a known polarization efficiency, they have modeled how the p-A_V relationship depends on the ratio of uniform to nonuniform fields, assuming perfect grain alignment. When applied to a data set composed of very diverse lines of sight through the ISM, the Jones/JKD model can successfully predict a global p_K-A_V relationship for the Milky Way.

The Jones/JKD model succeeds, in part, because of how the data were selected. The data sets used by Jones (1989) and JKD contain a considerable number of stars with very high polarizations ($5\% < p_K < 20\%$) at large optical depths ($20 < A_V < 100$ mag), indicating a high polarizing efficiency for these heavily extinguished lines of sight. As Figure 7 shows, this degree of polarizing efficiency is not found for lines of sight through cold dark clouds. Careful examination of the lines of sight tabulated in Jones (1989) and JKD shows that the high optical depth lines of sight are either in the diffuse ISM (e.g., toward the Galactic center) or toward luminous stars embedded in warm cloud cores in massive star-forming regions (e.g., BN). There are very few stars that are background field stars shining through a very opaque region in a cold dark cloud. This is clearly a selection effect, since the odds of a luminous background field star being directly behind a very opaque region in a cold dark cloud are low. If a statistically significant number of such stars could be found, our results at lower extinctions suggest there would be no additional polarization due to the intervening cold dark cloud. If many such stars were added to the polarization-extinction plots in Jones (1989) or JKD, our arguments in this paper would predict that the low-polarization high-extinction region of parameter space would be filled in, making the correlation derived from the selection-biased data look more like an upper limit.

Very recently, this prediction has been borne out. Creese, Jones, & Kobulnicky (1995) carried out a near-infrared polarization survey of the anomalously reddened stars cataloged by Stephenson (1992). The majority of these stars acquire their large reddening by virtue of being behind truly overdense gas in the ISM, and not just by being far away (as was often the case in the Jones/JKD sample). Creese et al. find an increase in p with A_V in their sample of reddened stars, but the increase is *significantly less than expected* based on the Jones/JKD model. They find they need to modify the Jones/JKD model to include regions with "bad grains," as suggested in this paper (§ 4.2), in order to predict the observed (approximately constant) percentage polarization.

Thus, the success of the Jones/JKD model in explaining the p-A_V relation for the Milky Way comes in large part from the fact that variations in polarization efficiency due to changing grain distributions average out when a range of conditions as wide as that considered by Jones and collaborators is included. Changes in polarization efficiency appear to matter most when a region of anomalously low polarization efficiency (e.g., a cold dark cloud) contributes most of the extinction along the line of sight (see Fig. 10 below).

4.1.2. p-A_V in Dark Clouds

In spite of all of the physical processes (changes in field orientation, field tangling, variations in grain alignment, variations in particle size, etc.) which serve to foul a simple positive correlation between polarization and extinction, many astronomers over the past 40 years have sought to find such correlations in individual regions, including several dark clouds. Usually, no tight correlation is found, and the slope of a linear fit to the data points is well below the upper bound shown in Figure 9. In Paper I, which presented the first p_K-A_V relation for a filamentary cold dark cloud, we noted that a weighted fit to the p_K-A_V data for B216-217 gives ~ 0 slope, but we were hesitant to stress this point. Now, however, having observed a second filamentary dark cloud (L1755) and again finding $p_K \propto A_V^{\sim 0}$ (Table 3), we are more confident in our claim that filamentary cold dark clouds show virtually no increase in percentage polarization with extinction over the range $1 < A_V < 10$ mag. In more bloblike, warmer dark clouds, such as the core of Ophiuchus (Wilking et al. 1979), Figure 7 shows that the increase in polarization with extinction is very gradual, with $p_K \propto A_V^{\sim 0.07}$ over the range $1 < A_V < 40$ mag (§ 3.3.2). For comparison, note that the upper envelope ($p_V = 3A_V$) shown in Figure 9 would have a slope of approximately 0.48% mag^{-1} in the p_K-A_V coordinate system used in Figure 7,[8] which is almost a full order of magnitude larger than the slopes listed for the "blobs" in Table 3.

The solid lines in Figure 7 show predictions of the Jones (1989) and JKD models for polarization as a function of extinction. As discussed in § 4.1.1, in these models each polarizing grain is assumed to polarize light equally well, and the depolarizing effects of field nonuniformity are used to account for the observed Galactic p_K-A_V relationship. The lines shown in Figure 7 assume that the nonuniform field energy is similar to the uniform field energy because this (equi)partition of field energy gives the best fit to the Milky Way data in JKD. Clearly, this model is not a good representation of the data for the filamentary clouds, and it represents, at best, an approximate upper bound to the data for bloblike dark clouds. In addition, the JKD model predicts narrowing of the distribution of polarization position angle as extinction increases, which is not observed in B216-217 or L1755: the distributions of optical and near-infrared polarization position angle have the *same* disperson for the same cloud, despite the sensitivity of optical and near-infrared observations to different extinction regimes (see Fig. 2 and § 3.1). Such narrowing *is* observed along some of the lines of sight included in the JKD study, but the optical polarization measurements in elongated dark clouds included in JKD notably do not follow the trend set by the other lines of sight in the sample. As suggested above, the Jones/JKD model is best used for predicting polarization-extinction relations along lines of sight where most of the extinction is produced by grains with a single representative distribution of polarization efficiencies, such as long lines of sight where high values of extinction are due entirely to increased path length, rather than an extreme local maximum density along the line of sight (e.g., a dark cloud).

4.2. *Which Grains Polarize What?*

4.2.1. *Clues from the Wavelength Dependence of Polarization and Grain Models*

The wavelength dependence of polarization can be understood in the context of theories which allow the estimation of the extinction, absorption, and scattering properties of materials of a known refractive index and shape. The details of the theory necessary to match the $p(\lambda)$ data (including the ideas that there are no aligned particles below a certain cutoff) are somewhat controversial, and they are beyond the scope of this

[8] This conversion assumes a wavelength of maximum polarization of 0.6 μm.

paper (see Spitzer 1978; Rogers & Martin 1979; Mathis 1986; Whittet 1992; Wolff et al. 1994; Kim & Martin 1994). The essential elements of the theory to appreciate here are: (1) *polarizing* effectiveness depends on the *difference* of extinction cross sections along principal grain axes; (2) the amount of *extinction* produced by a grain depends on the *sum* of extinction cross sections along principal axes; (3) the ratio of *polarization to extinction* for a particular grain depends on the *ratio* of this difference and this sum; and (4) the cross sections themselves depend on only the effective index of refraction and on $x = 2\pi a/\lambda$, where a is the characteristic grain size and λ is the wavelength of the incident light.

Figure 3 shows the size dependence of the polarization-to-extinction ratio for a single grain. The "extinction efficiency factors" for grains whose long axes are parallel to the electric or magnetic vectors of the incident radiation, denoted in Figure 3 as Q_{eE} and Q_{eH}, respectively, are each just the ratio of the extinction cross section for the relevant orientation to the geometric cross section. The total extinguishing power of a grain is proportional to $Q_{eE} + Q_{eH}$, whereas the polarizing power of a grain is proportional to $Q_{eH} - Q_{eH}$. As is immediately apparent from Figure 3, some grains polarize light far more efficiently than others. Note that the polarizing efficiency of a single grain is less sensitive to grain size at longer wavelengths. Also note that a major fraction of the extinction at all wavelengths is due to grains that are not part of the population of grains that can polarize light effectively. In other words, not all grains which produce significant extinction will produce significant polarization.

Typically, the number distribution of grain sizes derived from modeling the wavelength dependence of extinction by interstellar dust goes roughly as $a^{-3.5}$ (Mathis, Rumpl, & Nordsieck 1977; see Kim, Martin, & Hendry 1994 for more detailed models of this distribution). In this steep power-law distribution—which is a good first-order fit for random line of sight through the ISM—the large grains which appear to have very high polarizing efficiency in Figure 3 are extremely rare.

Our polarimetric results in the dark clouds B216-217 and L1755, which show no increase in percentage polarization associated with increasing extinction lead us to specifically conclude that most of the grains in cold dark clouds are very inefficient at polarizing near-infrared background starlight. This inefficiency could be due, at least in part, to an increase in grain size, but in order to calculate in detail which grains are responsible for the observed polarization at a given wavelength along a particular line of sight, one must take into account not only the grain size distribution along that line of sight, but also the grains' shapes and compositions, the details of the grain alignment mechanism, and the local orientation of the aligning magnetic field. Table 4 outlines the considerations necessary to evaluate how much polarization will be produced by a particular grain along a particular line of sight.

It is not a new idea that only certain grains are good at polarizing light. Several researchers before us, have emphasized that, "there may be entire populations of grains which contribute only to the extinction because they are not aligned or not elongated" (Clayton & Mathis 1988, p. 911). One of the main motivations for Mathis's very successful super-

TABLE 4

SOME FACTORS DETERMINING THE POLARIZATION OF BACKGROUND STARLIGHT

Size	Grains with size $a \sim \lambda/2\pi$ are most effective at polarizing background starlight of wavelength λ. Much larger and much smaller grains contribute significant extinction but not much polarization (see Spitzer 1978; Whittet 1992; Wolff et al. 1994).
Shape	Only substantially elongated grains will contribute polarization.
	Oblate grains polarize differently than prolate grains.
	Grains become rounder if mantles form, as can happen in dense cold regions when ices condense on the surfaces of grains (Eiroa & Hodapp 1989; Vrba et al. 1993; Whittet et al. 1988).
	Physically distinct grain formation mechanisms, such as coagulation (e.g., Mathis & Whiffen 1989; Wolff et al. 1994) and accretion (Aannestad 1982; Aannestad & Greenberg 1983) will favor different grain geometries.
Composition	Empirical results show that metallic (e.g., graphitic and amorphous carbon) particles can contribute significant extinction, but virtually no polarization. This means polarizing grains are necessarily a subset of all grains.
	Index of refraction depends on chemical composition and physical structure (i.e., fractal or fluffy vs. solid grains) of grains, even for silicates. The width of wavelength dependence of polarization curve increases as grains become more porous (Wolff et al. 1994). Dust particles' composition depends on how, when, and where they were formed.
Alignment	Thermal spin goes to zero in regions with no gas/grain temperature difference (i.e., dark clouds).
	Suprathermal spin (Purcell 1979) is diminished significantly in absence of atomic hydrogen, if recombination on grain surfaces is primary driver.
	Superparamagnetic (SPM) inclusions may be necessary to facilitate grain alignment, and in the SPM alignment model of Mathis 1986, grains smaller than a particular radius ($\sim$0.090 μm for the lines of sight sampled by Wilking et al. 1982 will not contain any SPM inclusions and will thus not be aligned.
	If de-aligning collisions are too frequent, compared to alignment time, alignment efficiency is reduced.
Magnetic field structure	Percentage polarization observed depends on inclination of field with respect to the line of sight. It is at a maximum for a field in the plane of the sky, and zero for a field exactly along the line of sight.
	Highly tangled field along a line of sight will reduce polarization observed. If, however, all grains are aligned, then polarization should still increase with extinction, due to random-walk–style arguments (Jones 1989; JKD).

paramagnetic grain alignment model (1986) was the fact that the extinction in the ultraviolet keeps rising while the polarization falls, implying that small grains contribute extinction there, but no polarization.

4.2.2. *Diminished Polarization Efficiency in Dark Clouds*

We do not wish to speculate here on which of the factors listed in Table 4 is *the* culprit in dark clouds—especially since a conspiracy among factors like these is probably in effect in these regions. Others, though, have made good arguments about specific deficiencies in dark clouds as causes of diminished polarization efficiency. For example, Vrba et al. (1993), and many others, have suggested, based on increased mean values of λ_{max}, that grains in cold dark clouds are preferentially larger and/or rounder than in other regions, which reduces the amount of polarization produced for a given amount of extinction. This argument is reasonable given that when observing at a given wavelength, only certain correctly sized (see Fig. 3) grains will effectively polarize background starlight, so a gross shift in grain size could render some grains essentially invisible from the point of view of the light that seeks to become polarized. Whether a shift large enough to explain the observed inefficiency of polarization is produced in dark clouds is, however, a question in need of further analysis (Goodman 1995a). Along another line of argument, Johnson (1982) and others have pointed out that the paucity of atomic hydrogen necessary to drive the spin-up process necessary to align grains (Purcell 1979) will cause poor grain alignment in very dense molecular clouds. Yet, strongly polarized emission, which presumably emanates from aligned grains in very dense molecular clouds *is* seen in far-infrared and submillimeter observations (see § 4.3), making the "poor alignment in dense regions" argument somewhat problematic.

Even without pointing the finger of blame at specific culprits, a general consideration of the theoretical requirements for the production of polarization, in conjunction with an understanding of the range of grain types known to exist in the ISM, leads directly to the conclusion that only a small subset of interstellar grains causes the polarization of background starlight. Figure 10*a* is intended as a schematic illustration of the grain distribution along the line of sight through a dark cloud containing a deficit of polarization-producing grains. In the figure, grains which produce substantial polarization of background starlight are rare, and are located preferentially *outside* the dark cloud region. Many other types of grains, both inside and outside of the dark cloud, produce substantial extinction.

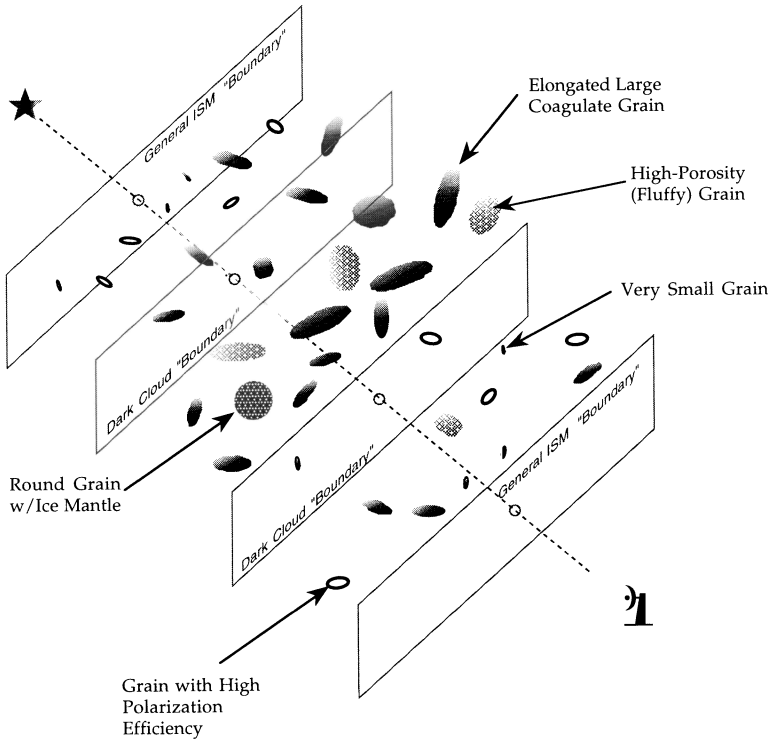

FIG. 10*a*

FIG. 10.—(*a*) Schematic diagram of grains in the ISM along a line of sight through a dark cloud to a background star. Many different grain types are present, but only some, which are shown as white with black outlines, produce the polarization of background starlight observed. These "polarizing" grains plus many others (shown as varying shades of gray) produce the extinction associated with the dark cloud. Notice that the dark cloud region shows a paucity of polarizing grains. (*b*) Changes in the efficiency of polarization caused by a grain distribution like the one envisioned in (*a*). The gray scale in the top panel shows a hypothetical distribution of extinction along a line of sight through a dark cloud. The plots in the middle two panels show particle density and polarizing efficiency, as a function of distance from the observer, assuming the extinction distribution in the top panel. In this hypothetical scenario, the drop in polarizing efficiency associated with the dark cloud produces a polarization-extinction relation similar to that sketched in the bottom panel. The question mark illustrates that we do not know the exact shape of this relation, and that we expect it to vary from region to region.

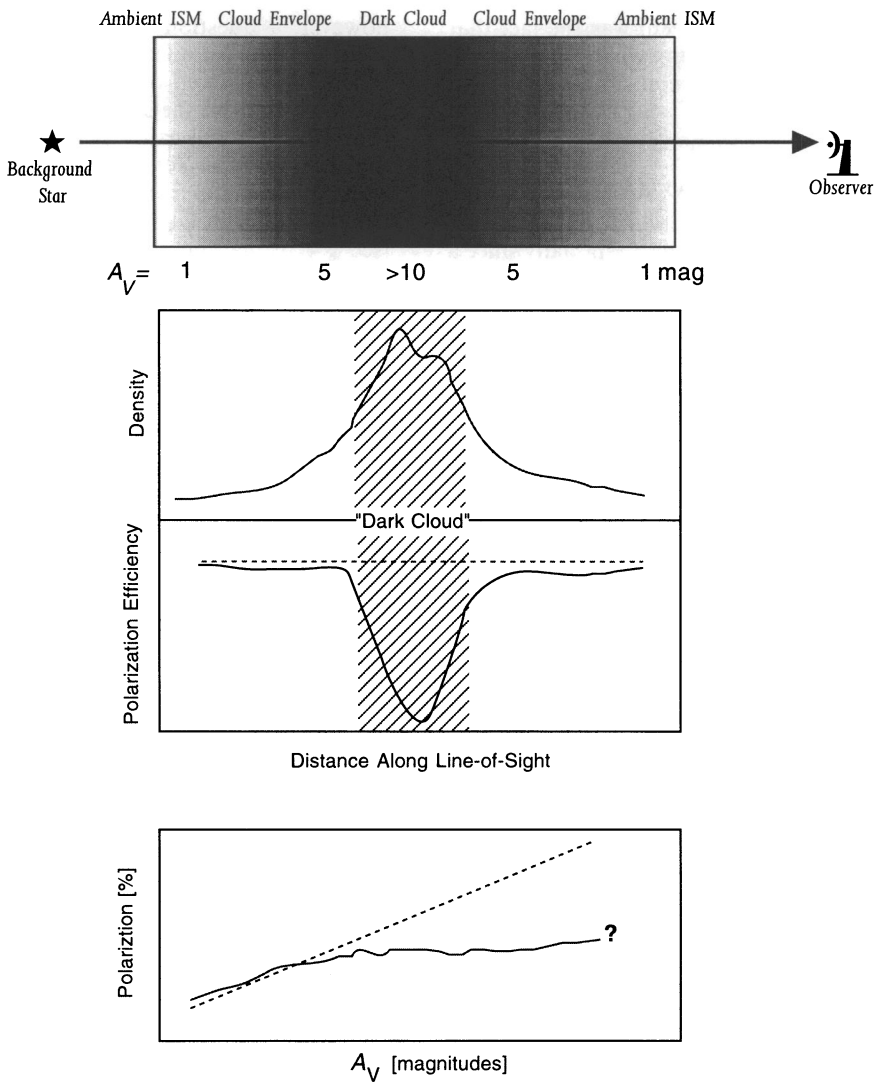

4.2.3. *Scenario for Polarization of Background Starlight Seen "through" Dark Clouds*

In Figure 10*b*, we present a schematic model for the polarization of background starlight along a line of sight through a dark cloud. This macroscopic view of the situation pictured in Figure 10*a* shows that the regions producing the most extinction are not the regions producing most of the polarization. The details of where, exactly, most of the polarization is produced are still unclear. It may be that an "envelope" of gas where the gas density is still higher than the ambient gas, but much lower than the densest part of the dark cloud, contains grains which polarize efficiently enough to produce most of the polarization on lines of sight through dark clouds. Or it may be that some much larger region, possibly as large as a whole molecular cloud complex, or larger, is producing most of the polarization. One way to distinguish between these alternatives is to survey large cloud complexes and search for changes in polarization percentage *and* position angle associated with density enhancements. The smallest scale on which such changes are seen will presumably correspond the highest density region that still contains enough polarizing grain to contribute substantially to the polarization of background starlight observed. The results of this paper and Paper I have shown us that the scale must be larger than the size of the filamentary dark clouds B216−217 and L1755 (approximately several parsecs) in dark cloud complexes such as Taurus and Ophiuchus.

The dark cloud known as the Coalsack provides an interesting test of the scenario illustrated in Figure 10*b*. Perhaps the only observational evidence that grains in cold dark cloud cores might be aligned and polarizing background starlight was the polarimetry of stars shining through Bok globule 2 in the Southern Coalsack (Jones et al. 1984). Jones et al. (1984) found that there was a clear rotation in position angle between the line of sight through the globule and the more diffuse region to the north. They interpreted this to imply that the grains in the globule itself were polarizing light. This result has subsequently been used by several authors (e.g., Klebe & Jones 1990) as "proof" that cold dense cores contain polarizing grains. However, careful examination of the observations of Bok globules by Jones et al. (1984) and Klebe & Jones (1990) reveals that there is *no increase in percentage polarization with extinction.* In addition, Bok globule 2 in the Southern Coalsack remains the *only* clear example of a rotation in position angle

coincident with a cold dark cloud core. It could very well be that the coalsack results are due not to grains deep within the globule, but due to grains that, while still part of the Southern Coalsack, are in front or behind the dense cloud core and by chance have a different alignment direction than the grains to the north of the Bok globule.

If we can learn the true shape of the density and polarization efficiency profiles shown schematically in Figure 10*b*, then we may be able to perform the deconvolutions necessary to understand what fields, where, lead to an observed polarization map of background starlight.

4.3. *Future of Magnetic Field Mapping in Dark Clouds*

4.3.1. *Polarized Thermal Emission from Dust*

It is now apparent that much of the polarization we see associated in projection with dense regions may not actually be produced there. While this is a disheartening thought in light of what it means for polarization maps of background starlight, a similar thought actually provides hope for more accurately measuring magnetic field structure in the future: the grains which produce the most polarization of background starlight (polarization seen in *absorption*) are not necessarily the same ones producing most of the polarization seen in thermal *emission* from grains. Thus, *observations of the polarized thermal emission from magnetically aligned dust in dense regions may still reveal the magnetic field there.*

Aligned grains which polarize light from background stars do so by having a slightly larger absorption cross section along their long axis than their short axis (see § 3.2.1), and the efficiency with which aligned grains produce polarization is only appreciable for a restricted range of grain sizes at a particular wavelength (Fig. 3). The aligned grains which do efficiently polarize background starlight will also *emit* polarized thermal radiation (see Dennison 1977; Hildebrand 1988; Novak et al. 1989; Stein 1966). However, other grains, which may be far from the peaks shown in Figure 3, can also easily produce polarized thermal radiation, because once x is less than about 0.1, cross sections for grains are determined by a dipole approximation and a wavelength-dependent index of refraction, which are not so sensitive to the ratio of grain size to wavelength as are the cross sections relevant to the case where $x \sim 1$ (Draine & Lee 1984). In fact, the wavelength dependence of the index of refraction (i.e., the dielectric constant) will cause larger grains, which may polarize very poorly in transmission, to be weighted more heavily in the polarization observed at the longer far-infrared and submillimeter wavelengths. The overall importance of this effect hinges on the size distribution of polarizing grains.

If different grains are responsible for producing the lion's share of the polarization seen in absorption than in emission, then it is possible that the polarization of background starlight and polarized emission from dust in a dense cloud would not imply the same magnetic field configuration (see Goodman 1995a, b). The Kuiper Airborne Observatory (KAO) has been used by many investigators to map out the polarization of thermal far-infrared and/or submillimeter dust emission in several dense clouds in the Galaxy (see Hildebrand et al. 1995; Davidson et al. 1995; Novak et al. 1989), including Orion (Gonatas et al. 1990; Hildebrand, Dragovan, & Novak 1984), the Galactic center (Hildebrand et al. 1990; Werner et al. 1988), W3, W51, and M17 (Dotson 1995). In one or two cases, background starlight polarimetry and far-infrared emission polarimetry seem to imply the same magnetic field direction (e.g., Orion), although the comparison often involves a handful of far-infrared measurements being compared with background polarimetry at the periphery of a heavily obscured region, up to $\sim 1^\circ$ away on the sky. In other cases (e.g., Mon R2; Novak et al. 1989), though, the two techniques clearly disagree in the direction they would ascribe to the magnetic field.

To date, the best place to compare emission and absorption polarimetry is M17, where recent detailed far-infrared (100 μm) polarization mapping (Dotson 1995) can be compared with new near-infrared (Goodman, Jones, & Myers 1995) and published optical (Schulz et al. 1981) observations of the polarization of background starlight. Initial comparisons of these data show a widely varying level of agreement between the emission and absorption polarimetry. Since M17 is 2.2 kpc away and very heavily extinguished, it is reasonable to hypothesize that the far-infrared polarization (and implied field structure) are legitimately associated with M17, while the background polarimetry is primarily representative of lower density regions along the (very long) line of sight to M17 (Goodman et al. 1995).

Polarization measurements of thermal emission from dust at millimeter and submillimeter wavelengths can sample the magnetic field in very cold dense regions (which may become optically thick at the shorter far-infrared wavelengths), and such measurements have recently begun to produce useful views of magnetic field structure (Leach et al. 1991; Minchin & Murray 1995; R. Akeson, J. Carlstrom, & J. A. Phillips 1994, private communication).

4.3.2. *Questions for the Future*

Most of the many questions this paper leaves unanswered stem from our lack of knowledge of the exact distribution of grain types and grain alignment in different regions of the ISM (Table 4). We know that some grains produce more polarization than others, relative to the amount of extinction they produce, but we do not know exactly which grains are where or exactly how much better one grain is at polarizing than the next. Is there meaning in the difference in the polarization efficiency found in the dense high-extinction bloblike dark clouds and the lower extinction, less dense, filamentary dark clouds? Do blobs contain a different grain distribution than filaments? Are conditions for grain alignment or grain growth better in one regime than the other? Do those conditions vary from cloud to cloud? These questions need answers if we are to understand not only polarization maps but also the details of the extinction and emission produced by interstellar dust in the dense ISM. Furthermore, if far-infrared and submillimeter polarimetry are to be the techniques of choice for mapping magnetic fields in the future, we must seek a better understanding of the production mechanism(s) for the polarization at those wavelengths.

5. CONCLUSIONS

5.1. *Summary*

We have mapped the polarization of near-infrared background starlight in the region associated with the dark cloud L1755. The pattern of polarization vectors does not show any change associated with the density enhancement represented by the dark cloud. The distribution of polarization position angles at optical and near-infrared wavelengths are virtually identical, despite the fact that the optical measurements sample lower density lines of sight around the periphery of the dark

cloud and near-infrared measurements sample higher density lines of sight *through* the dark cloud. In the dark cloud B216-217 (Paper I), we find entirely similar results: optical and near-infrared polarimetry are indistinguishable, and the dark cloud appears to have no effect on the pattern of polarization vectors.

In both L1755 and B216-217, the percentage of near-infrared polarization is not seen to increase with extinction. This result, combined with the clouds' apparent lack of effect on the angular distribution of the polarization vectors, leads us to the conclusion that while dark clouds like L1755 and B216-217 produce prodigious extinction, they do not produce much polarization. Therefore, the polarization measured is not a good representation of the magnetic field "inside" these dark clouds.

Results from the polarimetry literature, combined with our own results in dark clouds, show that, in general, polarization does not correlate well with extinction in individual regions. The relationship between polarization and extinction is heavily dependent on magnetic field geometry, but at high extinction, geometry alone cannot explain why the theoretical maximum polarization is never observed. We hypothesize that the lack of correlation, and diminished polarization efficiency at high extinction, are due to the fact that certain grains are much better at polarizing background starlight than others, relative to their capacity to produce extinction. If one samples long lines of sight with a diverse mix of grain types, polarization will rise with extinction, and the field structure deduced from polarization maps will be representative of the plane-of-the-sky field averaged over the whole line of sight to the background star. If, however, one samples a region where most grains are particularly inept at polarizing light, polarization will not increase systematically with extinction, and the magnetic field structure deduced will not be representative the region with these "bad" grains. For example, if a dark cloud contains many grains "good" at extinguishing light and "bad" at polarizing it, maps of polarization in dark clouds do not reveal the field there.

Analysis of the wavelength dependence of polarization reveals a large range of λ_{max} in L1755. This range is indicative of substantial variations in grain properties among neighboring lines of sight.

Considering background starlight polarimetry's potential for producing misleading maps of magnetic field structure in dense regions of the ISM, we reflect on the utility of mapping the polarization of thermal emission from grains as an alternative. The variations in grain properties responsible for the "weighting" of background starlight polarimetry may not be as much of a problem in emission polarimetry.

5.2. *Does Near-infrared Polarimetry Reveal the Magnetic Field in Cold Dark Clouds?*

No. It is probably not wise to accept background starlight polarization observations of isolated dark clouds which show no rise in percentage polarization with extinction as reliable portrayals of the magnetic field structure in those clouds.

We are grateful to Carl Heiles for useful comments on grain absorption, emission, and scattering properties, to Mike Wolff and Geoff Clayton for a useful preprint on fluffy grains, to Charlie Lada for illuminating discussions on extinction curves, to Bruce Draine for useful suggestions and calculations, to David Wilner for his thoughtful comments, and to Dan Clemens, Gary Fuller, Lincoln Greenhill, Diego Mardones, John Mathis, Edward Schwartz, Steve Strom, Boqi Wang, and Doug Whittet for their valuable input. We thank Mark Creese for assisting with the IRTF observing. A. A. G. is grateful to Danny, of the Stanford University Bookstore, and Apple Computer for fixing her dead laptop computer in 2 hours on a layover in San Francisco, which allowed for real-time analysis of the IRTF data in this paper. T. J. J. acknowledges support for MIRP frm NSF grant AST 8912803. E. A. L. acknowledges support from a Hubble Grant through HF1047.01-934 from STScI to the University of Maryland.

REFERENCES

Aannestad, P. A. 1982, A&A, 115, 219
Aannestad, P. A., & Greenberg, J. M. 1983, ApJ, 272, 551
Chandrasekhar, S., & Fermi, E. 1953, ApJ, 118, 116
Clayton, G. C. & Mathis, J. S. 1988, ApJ, 327, 911
Creese, M., Jones, T. J., & Kobulnicky, A. 1995, ApJ, submitted
Davidson, J. A., Dowell, C. D., Schleuning, D., Dotson, J., & Hildebrand, R. H. 1995, in From Gas to Stars to Dust, ed. J. Davidson, E. Erickson, & M. Haas (San Francisco: ASP), in press
Davis, L., Jr., & Greenstein, J. L. 1951, ApJ, 114, 206
Dennison, B. 1977, ApJ, 215, 529
Dickman, R. L. 1988, in Lecture Notes in Physics, 315, Molecular Clouds in the Milky Way and External Galaxies, ed. R. L. Dickman, R. L. Snell & J. S. Young (Berlin: Springer), 55
Dotson, J. 1995, ApJ, in press
Draine, B. T., & Lee, H. M. 1984, ApJ, 285, 89
Eiroa, C., & Hodapp, K.-W. 1989, A&A, 210, 345
Fowler, A. M., et al. 1987, Opt. Eng., 26, 232
Garwood, R., & Jones, T. J. 1987, PASP, 99, 453
Gonatas, D. P., et al. 1990, ApJ, 357, 132
Goodman, A. A. 1995a, ApJ, in preparation
———. 1995b, in Airborne Astronomy Symp. on the Galactic Ecosystem: From Gas to Stars to Dust, ed. M. Haas, J. Davidson, & E. Erickson (San Francisco: ASP), 45
Goodman, A. A., Bastien, P., Myers, P. C., & Ménard, F. 1990, ApJ, 359, 363
Goodman, A. A., Jones, T. J., Lada, E. A., & Myers, P. C. 1992, ApJ, 399, 108 (Paper I)
Goodman, A. A., Jones, T. J., & Myers, P. C. 1995, in preparation
Hall, J. S. 1949, Science, 109, 166
Hall, J. S., & Mikesell, A. H. 1949, AJ, 54, 187
———. 1950, Publ. US Naval Obs., 17, Table IV
Heyer, M. H., et al. 1987, ApJ, 321, 855
Hildebrand, R. H. 1988, QJRAS, 29, 327
Hildebrand, R. H., et al. 1995, in From Gas to Stars to Dust, ed. J. Davidson, E. Erickson, & M. Haas (San Francisco: ASP), in press
Hildebrand, R. H., Dragovan, M., & Novak, G. 1984, ApJ, 284, L51
Hildebrand, R. H., Gonatas, D. P., Platt, S. R., Wu, X. D., Davidson, J. A., & Werner, M. W. 1990, ApJ, 362, 114
Hiltner, W. A. 1949a, ApJ, 109, 471
———. 1949b, Science, 109, 165
———. 1950, Phys. Rev., 78, 170
———. 1956, ApJS, 2, 389
Hodapp, K.-W. 1984, A&A, 141, 255
———. 1987a, A&A, 172, 304
———. 1987b, ApJ, 319, 842
———. 1990, ApJ, 352, 184
Johnson, P. E. 1982, Nature, 295, 371
Jones, T. J. 1989, ApJ, 346, 728
Jones, T. J., Hyland, A. R., & Bailey, J. 1984, ApJ, 282, 675
Jones, T. J., & Klebe, D. I. 1988, PASP, 100, 1158
Jones, T. J., Klebe, D., & Dickey, J. M. 1992, ApJ, 389, 602 (JKD)
Kim, S.-H., & Martin, P. G. 1994, ApJ, 431, 783
Kim, S.-H., Martin, P. G., & Hendry, P. D. 1994, ApJ, 422, 164
Klebe, D. I., & Jones, T. J. 1990, AJ, 99, 638
Lada, E. A., DePoy, D. L., Evans, N. J., II, & Gatley, I. 1991, ApJ, 371, 171
Leach, R. W., Clemens, D. P., Kane, B. D., & Barvainis, R. 1991, ApJ, 370, 257
Loren, R. B. 1989, ApJ, 338, 902
Martin, P. G., & Whittet, D. C. B. 1990, ApJ, 357, 113
Mathewson, D. S., Ford, V. I., & Krautter, J. 1978, CDS Bull., 14, 115
Mathis, J. 1986, ApJ, 308, 281
Mathis, J. S. 1990, ARA&A, 28, 37
Mathis, J. S., Rumpl, W., & Nordsieck, K. H. 1977, ApJ, 217, 425
Mathis, J. S., & Whiffen, G. 1989, ApJ, 341, 808
Minchin, N. R., & Murray, A. G. 1995, A&A, in press
Moneti, A., Pipher, J. L., Helfer, H. L., McMillan, R. S., & Perry, M. L. 1984, ApJ, 282, 508
Myers, P. C., & Goodman, A. A. 1991, ApJ, 373, 509 (MG)
Novak, G., Gonatas, D. P., Hildebrand, R. H., & Platt, S. R. 1989, ApJ, 345, 802

Purcell, E. M. 1979, ApJ, 231, 4404
Rogers, C., & Martin, P. 1979, ApJ, 228, 450
Sato, S., et al. 1988, MNRAS, 230, 321
Schulz, A., Lenzen, R., Schmidt, T., & Proetel, K. 1981, A&A, 95, 94
Serkowski, K. 1974, in Methods of Experimental Physics, ed. N. Carleton (New York: Academic)
Serkowski, K., Mathewson, D. S., & Ford, V. L. 1975, ApJ, 196, 261
Spitzer, L., Jr. 1978, Physical Processes in the Interstellar Medium (New York: Wiley)
Stein, W. 1966, ApJ, 144, 218
Stephenson, C. B. 1992, AJ, 103, 263
Tamura, M., Nagata, T., Sato, S., & Tanaka, M. 1987, MNRAS, 224, 413
Tamura, M., Yamashita, T., Sato, S., Nagata, T., & Gatley, I. 1988, MNRAS, 231, 445
Vrba, F. J., Coyne, G. V., & Tapia, S. 1981, ApJ, 243, 489
Vrba, F. J., Coyne, G. V., & Tapia, S. 1993, AJ, 105, 1010
Werner, M. W., Davidson, J. A., Morris, M., Novak, G., & Platt, S. R. 1988, ApJ, 333, 729
Whittet, D. C. B. 1992, Dust in the Galactic Environment (Bristol: IOP)
———. 1995, in The Cosmic Dust Connection, ed. J. M. Greenberg (Dordrecht: Kluwer), in press
Whittet, D. C. B., et al. 1988, MNRAS, 233, 321
Whittet, D. C. B., Martin, P. G., Hough, J. H., Rouse, M. F., Bailey, J. A., & Axon, D. J. 1992, ApJ, 386, 562
Wilking, B. A., Lebofsky, M. J., Martin, P. G., Rieke, G. H., & Kemp, J. C. 1980, ApJ, 235, 905
Wilking, B. A., Lebofsky, M. J., & Rieke, G. H. 1982, AJ, 87, 695
Wilking, B. A., Lebofsky, M. J., Rieke, G. H., & Kemp, J. C. 1979, AJ, 84, 199
Wolff, M. J., Clayton, G. C., Martin, P. G., & Schulte-Ladbeck, R. E. 1994, ApJ, 423, 412